ISSN 1346-8901

PROCEEDING

HISAS 8

The 8th Hokkaido Indonesian Student Association Scientific Meeting

Multi-disciplinary Scientist as Indonesia Resources towards Society Welfare Equality and Sustainability

Sapporo, 6th February 2010

PREFACE

Concerning Indonesia's human resource development, Indonesia Student Association in Hokkaido (PPI Hokkaido) establishes a mission to support the Indonesian students who are studying in excellent universities in Hokkaido, Japan. Simultaneously, PPI Hokkaido encourages Indonesian students to give real contribution and get involved actively in Indonesia's development. In addition PPI Hokkaido annually holds a scientific meeting among Indonesian students in Hokkaido in order to increase the ability on problem-solving by gaining various knowledge from various field of studies, and to formulate an integrated approach from these various field of studies to offer an innovative solution for Indonesia's development.

This year PPI-H held this scientific meeting for the eighth time, with title "The 8th Hokkaido Indonesian Association Scientific Meeting (HISAS 8)". Adopting theme *Multi-Disciplinary Scientists as Indonesia Resources towards Society Welfare Equality and Environmental Sustainability*, newly acquired knowledge and proposed solutions on threat and challenges of Indonesian mega diversity were presented and discussed. Together with other important findings from engineering view this meeting showed that the multi disciplinary studies of Indonesian students in Hokkaido will give multiple benefit not only for self-development, but also for the social, welfare and environmental sustainability of Indonesia.

Appreciation goes to all of speakers for their contribution and to all of the organizing committees on their hard work for the success of this meeting. Sincere acknowledgments are extended to Indonesian Embassy for Japan, Hokkaido University and Hokkaido Gas Company (Kita Gas) for their support on this meeting. We do hope that results and findings discovered and gained from this meeting as well as the offered solutions can be implemented well, and harmonized with Indonesian government and policy to meet the Indonesian future challenges, not only to answer the environmental issues but also for developing the human building capacity in Indonesia.

Sapporo, 27th November 2010

Organizing Committee of HISAS 8
Chairman,

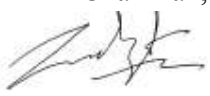

Erianto Indra Putra, Ph.D

CONTENT

List of Organizing Committee

Advisory board	:	Chairman of Indonesian Student Association of Hokkaido
		Chairman of Indonesian Student Association of Sapporo
Chairman	:	Erianto Indra Putra, Ph.D
Vice Chairman	:	Gun Gun Hidayat (*ex-officio*)
		Refi Ikhtiari (*ex-officio*)
Secretary	:	Aditya Gusman
Treasurer	:	Arya Utami
Paper Coordinator	:	Ali Sobirin
		Rudy Syahputra
		Ixchel Mandagi
		Anastasia Setiawan
Equipment	:	Eko Siswoyo
		Heri Kurniawan
Transportation	:	Hari Setiapraja
		Cholil
Documentation	:	Erwin Suwendi
		Euis Tintin Yuningsih
Food Supplies	:	Esti Puspitaningrum
		Indun Puspita
		Eni Sugiarti
Proposal & Program	:	Surya Kencana Joe
		Budi Hasiholan
		Teddy Eka Putra
		Mutiara Sidharta
Information and Website	:	Toto Sudiro
Public Relation	:	Gun Gun Hidayat
		Maria Stefanie Dwiyanti
Editorial Board	:	Ali Awaludin, Ph.D
		Yaya Rayadin, Ph.D

BIODIVERSITY OF BAGWORM (LEPIDOPTERA:PSYCHIDAE) ON ORNAMENTAL PLANT IN SOUTH SUMATERA, INDONESIA

Yulia Pujiastuti

PS Agro-ecotechnology, Faculty of Agriculture Sriwijaya University
Jln. Palembang-Prabumulih Km.32 Kampus Inderalaya Ogan Ilir South Sumatera
e-mail: yulunsri@yahoo.com

ABSTRACT: The purpose of research was to investigate biodiversity, population of bagworm and their parasites in South Sumatera, Indonesia. Survey was conducted in rainy and dry seasons, from October 2008 to August 2009. The method used was purposive sampling method, with ornamental plants grown in home yard, public garden and garden flower's seller as the targets. The observation covered: species of bagworm, number of bagworm exist on each ornamental plant, position of bagworm, form of bagworm's case, level of parasitization of bagworm and information of bagworm's control. Identification of bagworm species refered to Kalshoven (1981), Mitchell *et al*. (2001), and related articles about bagworm. Nine species of ornamental plants, i.e. Rose (*Rosa* sp), Orchid (*Dendrabium anosmum*), Asoka (*Ixora* spp.), Bougenvillia *(Bougenvillia spectabilis*), Hibiscus (*Hibiscus rosasinensis*), Euphorbia (*Euphorbia milli*), Palmae (*Hyophorbe lagenicaulis*), Roselle (*Hibiscus sabdariffa*), and Alamanda (*Allamanda cathartica*) were observed. All sampled plant species were grown in home yards, five species (rose, bougenvillia, hibiscus, asoka, palmae, and alamanda) were planted in public parks, and all ornamental plants -except roselle- were found in garden flower's seller. The species of bagworm associated with those ornamental plants were identified as *Pagodiella hekmeyeri* Heyl, *Clania variegata* Sn, *Chaliodes kondonis* Sn, *Oiketicus abotti* Templ, *Pteroma plagiophles* Hps, *Mahasena corbetti* Tams, and *Clania minuscula* Joannis. Population of *Pteroma plagiophles* was the highest both in rainy and dry seasons. Rose, bougenvillia and alamanda were attacked by three of bagworm species, hibiscus and euphorbia were attacked by four species of bagworm. Orchid, palmae, asoka and roselle were attacked by five species of bagworm. Position of bagworm in ornamental plants varied in parts of the tree such as leaves, trunk, branch and flower. Bagworms were easily identified by the form of their cases. Each species had its own type of case, such as *Chalioides kondonis* with its cone-shape case. Level of parasitization was low (0.00 – 18.54 percent). The rank of bagworm's number and species found was as follows: home yards, public parks and flower sellers. Controlling of the bagworms was done by mechanical hand picking. No chemical control was applied on these insects.

Keywords*: bagworms, ornamental plants, insect pests*

1. BACKGROUND

Ornamental plants are the keystone of ornamental gardening, and they come in a range of shapes, sizes and colors suitable to a broad array of climates, landscapes, and gardening needs. They also play an economically important role in agricultural commodities trade. Some ornamental plants are grown for showy foliage. Other ornamental plants are cultivated for their blooms. Flowering ornamentals are a key aspect of many gardens, with many flower gardeners preferring to plant a variety of flowers so that the garden is continuously in flower throughout the year. Other ornamental plants such as palmae most namely by evergreen trees.

Many species of insects attack ornamental plants, of which bagworm is a very important pest due to its specific type of attack symptom (Kalshoven, 1981). Not only on leaves this insects feed, but also on stem, branch and flowers. Bagworms usually begin feeding at the top of the tree. When small, the caterpillars feed in the layers of the leaf tissue, creating light patches on leaves. As they age, they consume entire needles or leaves. A severe infestation may defoliate plants, which can kill branches or entire plants. A healthy deciduous tree or shrub that has been defoliated usually produces a new flush of leaves and survives. However, a defoliated evergreen cannot push out an additional set of leaves and may die. As soon as the first showers signal the beginning of the rains the eggs hatch and hundreds of tiny caterpillars disperse from the mother bag. These caterpillars are naked to begin with but witin a few hours they have gathered enough leaf material for a small cone that can cover them. The material is taken from epidermis of the leaf but the damage is hardly visible. At this stage the cones are whitish or pale green. The attack is first noticed as small spots, scattered over the mopane leaves. The spots are about 5 mm in diameter and they eventually turn red-brown. Only the epidermis is eaten so there are no holes through the leaf. The small caterpillars can be found in small cone-shaped bags made of green leaf material. The caterpillars spend the rest of their life in such bags that just are expanded when the caterpillars grow bigger. They can move easily by strecthing their heads out through an opening in the top of the bag and pull the bag to a new place on the leaf. In particular it is estimated a modified Economic Injury Level (EIL) for the bagworm, *Thyridopteryx ephemeraeformis* (Haworth), attacking American arborvitae, *Thuja occidentalis* under retail nursery conditions. Under these circumstances, the Economic Injured Level (EIL) was found to be only about four first instar larvae per 4 ft tree (Raupp *et al*., 1989). In Indonesia thousands of sengon (Albizia) tree in Tambakroto, Kajen, Pekalongan District, severely attacked by bagworm. The farmers lossed the yield of those tree, and it decreased farmers' income because of bad qualified of the albizia wood (Antara News Agency, May 29, 2009). In the world, it is known 600 species of bagworm, but in Indonesia there is no report how many of species exist. In Sapporo, Japan, there is no report about bagworm living in this area (Kinota, 2006). In Western Japan, data reported by Nishida (1983), there were two species bagworm i.e. *Eumeta japonica* dan *Eumeta minuscula* (now namely *Clania variegatta*) are important pests of shade and ornamental trees and shrubs.There was no data reported on ornamental plants due to bagworm attack especially in South Sumatera. Therefore, this paper will report the results of research about bagworm on ornamental plants in South Sumatera.

2. MATERIALS AND METHOD

The research was conducted in two districts in South Sumatera i.e. Ogan Ilir and Palembang, using purposive sampling method in rainy and dry season (October 2008 - August 2009). Observations were held in home yard's garden, public garden and garden flower's seller. The target ornamental plants were Rose (*Rosa* sp), Orchid (*Dendrabium anosmum*), Asoka (*Ixora* spp.), Bougenvillia *(Bougenvillia spectabilis*), Hibiscus (*Hibiscus rosasinensis*), Euphorbia (*Euphorbia milli*), Palmae (*Hyophorbe lagenicaulis*), Roselle (*Hibiscus sabdariffa*), and Alamanda (*Allamanda cathartica*). Observation was covered: species of bagworm, number of bagworm exist on each ornamental plant, position of bagworm, form of bagworm's case, level of parasitization of bagworm and information of bagworm's control. At least 10 trees of target ornamental plants were observed. Observation were done twice, i.e. rainy season (October 2008 to March 2009) and dry season (April 2009 to August 2009). The species of bagworms, number of bagworm sampled, and parasitization of bagworm were noted. Parasitization was noted by opening the bagworm. The positions of bagworm on ornamental trees were documented.

3. RESULTS AND DISSCUSION

3.1 Biodiversity Species of bagworm

The observations conducted in dry and rainy seasons, found 944 individues of bagworm, identified as 7 species of bagworm: *Pagodiella hekmeyeri* Heyl, *Clania variegata* Sn, *Chaliodes kondonis* Sn, *Oiketicus abotti* Templ, *Pteroma plagiophles* Hps, *Mahasena corbetti* Tams, dan *Clania minuscula* Joannis. Number of each species of bagworm was shown in Table 1. The highest number of bagworm was *Pteroma plagiophles* Hps, both in rainy and dry season. This species was also found in several ornamental plants, it seemed that *P. plagiphles* was polyphagous insect. It was also reported by Jar and Sarma (2008) *P. plagiophles* was a cosmoplitan and polyhagous insect in India. Observation done in garden's house hold, public garden and garden flower's seller showed that symptom of bagworm attack was losses of epidermis part of leave, forming holes in many places. Leave will falling down easily and plants will loss the leaves.

Table 1. Biodiversity of bagworm on ornamental plants in South Sumatera in rainy and dry seasons

No	Host plant	Species of bagworm	Amount of individues	
			Rainy season	Dry season
1	Rose (*Rosa* sp.)	*Oiketicus abotti*	13	18
		Clania variegata	5	2
		Pteroma plagiophles	34	41
2	Orchid (*Dendrabium anosmum*)	*Clania variegata*	15	11
		Chaliodes kondonis	23	15
		Mahasena corbetti	2	-
		Oiketicus abotti	3	6
		Pteroma plagiophles	12	18
3	Bougenvillia *(Bougenvillia spectabilis*)	*Pteroma plagiophles*	35	32
		Mahasena corbetti	11	6
		Oiketicus abotti	8	3
4	Palmae (*Hyophorbe lagenicaulis*)	*Chaliodes kondonis*	5	6
		Pteroma plagiophles	13	45
		Clania minuscula	2	13
		Oiketicus abotti	12	3
		Mahasena corbetti	31	43
5	Hibiscus (*Hibiscus rosasinensis*)	*Oiketicus abotti*	8	2
		Chaliodes kondonis	16	19
		Clania variegata	3	7
		Pteroma plagiophles	6	15
6	Asoka (*Ixora* spp.)	*Pagodiella hekmeyeri*	-	13
		Chaliodes kondonis	3	25
		Oiketicus abotti	11	12
		Clania minuscule	2	8
		Pteroma plagiophles	27	17
7	Roselle (*Hibiscus sabdariffa*)	*Pteroma plagiophles*	19	28
		Mahasena corbetti	12	5
		Clania minuscula	2	15
		Clania variegata	-	7
		Oiketicus abotti	3	6
8	Alamanda (*Allamanda cathartica*)	*Clania variegata*	8	15
		Mahasena corbetti	11	20
		Chaliodes kondonis	-	30
9	Euphorbia (*Euphorbia milli*)	*Pteroma plagiophles*	18	27
		Oiketicus abotti	-	13
		Chaliodes kondonis	2	15
		Pagodiella hekmeyeri	-	8

3.2 Number of bagworm observed *in situ*

Number individues sampled were different between rainy season and dry season. It can be shown in Figure 1. In general, number of individues found in dry season much higher rather than in rainy season. It was predicted that suitable micro-climate will cause the reproduction process happened without any constraints. Mating occured between male and female and a lot of eggs (100-300 eggs) produced by females in her own pocket. Thus, the bagworm population grow faster in dry season than rainy season. When it was raining, rain's drop physically will effect the first instar of bagworm due to uncover body of those larvae.

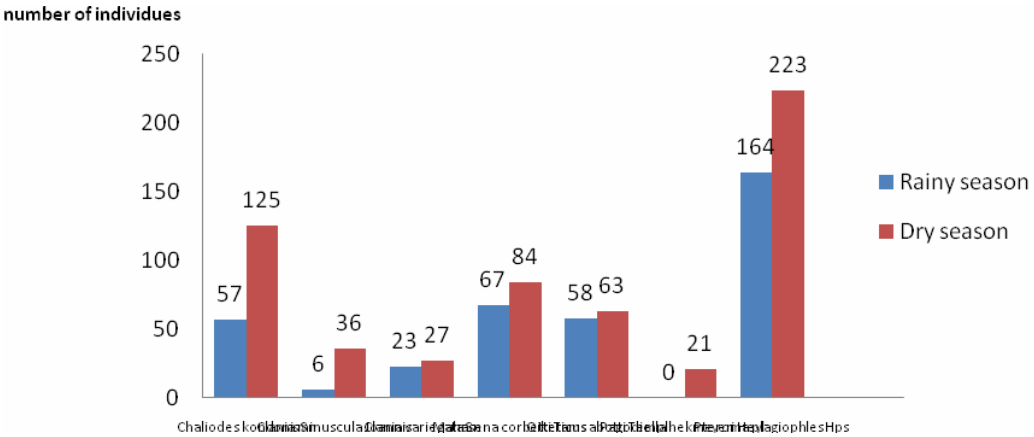

Fig. 1 Number of indvidues of each species of bagworm found in rainy and dry season in ornamental plants in South Sumatera, Indonesia

3.3 Biodiversity of ornamental plants as bagworm host

All target ornamental plant were attacked by bagworm in various instar. This report did not note specific instar attack, but interestingly, bagworm were found not only in young plant but also some years old plant. It is also noted that larvae found on leave (*Phaodiella hekmeyeri* and *Oiketicus abboti*) and on stem or branch (*C. kondonis*). The result also noted in a torny ornamental plant such as rose and euphorbia, the bagworm still alive and attack those plants. They make a bag from any dry leaves and compiled in a specific form. Bagworm form were specific in each species (Rhainds *et al*., 2009).

Bagworms were identified polyphagous and cosmopolitant insect. Table 2 showed 2 species of bagworms are polyphagous bagworms, namely *Oiketicus abotti* and *Pteroma plagiophles*. Both are attacking Rose (*Rosa* sp.) Orchid (*Dendrabium anosmum*), Bougenvillia (*Bougenvillia spectabilis*), Palmae (*Hyophorbe lagenicaulis*), Hibiscus (*Hibiscus rosasinensis*), Asoka (*Ixora* spp.), Roselle (*Hibiscus sabdariffa*), and Euphorbia (*Euphorbia milli*). There was a tendency of those species to adapt the part of plants they attacked.

Table 2. List of ornamental plants as the hosts of bagworm

No	Species of bagworm	Species of host plants
1	*Chaliodes kondonis* Sn	1. Orchid (*Dendrabium anosmum*) 2. Palmae (*Hyophorbe lagenicaulis*) 3. Hibiscus (*Hibiscus rosasinensis*) 4. Asoka (*Ixora* spp.), 5. Alamanda (*Allamanda cathartica*) 6. Euphorbia (*Euphorbia milli*)
2	*Clania minuscula* Joannis	1.Palmae (*Hyophorbe lagenicaulis*) 2.Asoka (*Ixora* spp.) 3.Roselle (*Hibiscus sabdariffa*)
3	*Clania variegata* Sn	1.Rose (*Rosa* sp.) 2.Orchid (*Dendrabium anosmum*) 3.Hibiscus (*Hibiscus rosasinensis*) 4.Roselle (*Hibiscus sabdariffa*) 5.Alamanda (*Allamanda cathartica*)
4	*Mahasena corbetti* Tams	1.Orchid (*Dendrabium anosmum*) 2.Bougenvillia *(Bougenvillia spectabilis*) 3.Palmae (*Hyophorbe lagenicaulis*) 4.Roselle (*Hibiscus sabdariffa*) 5.Alamanda (*Allamanda cathartica*)
5	*Oiketicus abotti* Templ	1.Rose (*Rosa* sp.) 2.Orchid (*Dendrabium anosmum*) 3.Bougenvillia *(Bougenvillia spectabilis*) 4.Palmae (*Hyophorbe lagenicaulis*) 5.Hibiscus (*Hibiscus rosasinensis*) 6.Asoka (*Ixora* spp.) 7.Roselle (*Hibiscus sabdariffa*) 8.Euphorbia (*Euphorbia milli*)
6	*Pagodiella hekmeyeri* Heyl	1.Asoka (*Ixora* spp.) 2. Euphorbia (*Euphorbia milli*)
7	*Pteroma plagiophles* Hps	1.Rose (*Rosa* sp.) 2.Orchid (*Dendrabium anosmum*) 3.Bougenvillia *(Bougenvillia spectabilis*) 4.Palmae (*Hyophorbe lagenicaulis*) 5.Hibiscus (*Hibiscus rosasinensis*) 6.Asoka (*Ixora* spp.) 7.Roselle (*Hibiscus sabdariffa*) 8.Euphorbia (*Euphorbia milli*)

3.4 Position of bagworm on ornamental plants and form of bagworm's case

In general bagworms attached their case on leaves. In this observation, four species (*C. kondonis, C. variegata, O. abotti*, and *P. plagiophles*) attached also on bark or stem of plants. *C.variegatta* attached also on flower of rose. Larvae took out its head from its case and feed in the layers of the leaf tissue, creating light patches on leaves. Larvae attached on stem and eat on bark of stem. Therefore they made their case from this part of trees. This position was very important to describe economically importance of a species. On albizia tree, the bagworm attach on bark and eat on it, consequently this part was severely damaged. Albizia's grower could not harvest the wood of albizia, therefore they could not get economically benefit (Antara News Agency, May 29, 2009).

There were many forms of bagworm's case. Each species had its own type of case, such as *Chalioides kondonis* with its cone-shape case. *M. corbetti* made their case in a spindle--

shaped bag, hanging by a rope from materials spun with its saliva. Some species make their case from pieces of foliage made based on the part of plant they live in. Forming of their cases can be determined their species.

3.5 Species and number of individues based on location they found

Observation of bagworms was conducted in three locations, i.e. home yards, public gardens and flower's seller. More than 50 percent of bagworms (55.83%) was found in homeyards, 29.24 percent in public gardens and 14.83 percent in flower's seller. This fact also showed that home yards owner did not take care the garden well, while in public parks, eventhough there were some officers did their job, the amount of bagworms found was higher than in flower's seller. The seller took care their ornamental plants very well because of their economically important commodities.

Table 3. Number of bagworm individues found in different locations

No	Species of bagworm	Number of individues		
		Home yards	Public parks	Flower's sellers
1	*Chaliodes kondonis* Sn	105	52	15
2	*Clania minuscula* Joannis	21	13	8
3	*Clania variegata* Sn	17	24	9
4	*Mahasena corbetti* Tams	96	42	13
5	*Oiketicus abotti* Templ	63	37	21
6	*Pagodiella hekmeyeri* Heyl	10	4	7
7	*Pteroma plagiophles* Hps	215	105	67
	Total	527 (55.83%)	277 (29.34%)	140 (14.83)

3.6 Parasitisation of bagworm

In this observation, it was observed whether the larvae were parasitized by parasitoid. Identification of parasitoid were on going. The result showed (Table 3) level of parasitization was ranged from 0.00 to 18.54 persen. The most parasitized bagworm was *Mahasena corbetti* (18.54 percent), and *Pteroma plagiophles* (13.69 percent). The level of parasitization was very low compare with thus on *Eumeta variegata* bagworm. This insect was an important insect pest on orchard and street trees in southwestern part of Japan. Newly invaded tachinid fly, *Nealsomyia rufella* reported as parasitised *E.variegatta* (Sawada and Arakawa, 2002). Level of parasitization on *E. variegata* bagworm by tachinid flies *Nealsomyia rufella* reached 96.4 percent. The percentage of parasitism ranged from 0 to 96.4% in each collection site, having a tendency to be higher in the urban area in the central part of Kochi.

Table 4. Level of parasitization of bagworm

No	Species of bagworm	Number of individues	Number of parasitised individues	% parasitization
1	*Chaliodes kondonis* Sn	182	5	2.74
2	*Clania minuscula* Joannis	42	2	4.76
3	*Clania variegata* Sn	50	0	0.00
4	*Mahasena corbetti* Tams	151	28	18.54
5	*Oiketicus abotti* Templ	121	8	6.61
6	*Pagodiella hekmeyeri* Heyl	21	0	0.00
7	*Pteroma plagiophles* Hps	387	53	13.69

3.7 Bagworm control

In the part of observation, bagworm control was asked to the owner of ornamental plants in home yards, officer in public parks and owner of flower's seller. The questions were about wheteher they knew about bagworms presence and how to control them. Out of 25 people who asked about the bagworms presence, 17 persons (68 percent) answered that they knew about bagworms and the rest (8 persons / 32 percent) said they did not understand what bagworms were. Among the people who knew bagworms, they controlled the bagworm directly by hand picking (13 persons / 76.45 percent) and the rest (4 persons / 23.55 percent) said they did not do anything. When they were asked whether they used chemical insecticides, they said that they never used for controlling bagworm.

4. CONCLUSIONS

All sampled plants were attacked by bagworm. Species of bagworm found in ornamental plants identified as *Pagodiella hekmeyeri* Heyl, *Clania variegata* Sn*, Chaliodes kondonis* Sn, *Oiketicus abotti* Templ*, Pteroma plagiophles* Hps*, Mahasena corbetti* Tams, dan *Clania minuscula* Joannis. *Pteroma plagiophles* was the highest number found in all ornamental plants. Each species had its own type of case Level of parasitisation was low (0.00 – 18.54 percent). The rank of bagworm's number and species found was as follows: home yards, public parks and flower seller. Controlling of the bagworms was done by mechanical hand picking. No chemical control was applied on these insects.

ACKNOWLEDGMENTS

The writer thanked to Ekasri Murniati and Merryska Gita Jayanti for supporting some data of bagworm species in some areas.

REFERENCES

Antara News Agency, 29 Mei 2009. Hama ulat kantong menyerang tanaman sengon(albizia). (in Indonesian)

Raupp, M. J., J. A. Davidson, C. S. Koehler, C. S. Sadof and K. Reichelderfer., 1989. Economic and Aesthetic Injury Levels and Thresholds for Insect Pests of Ornamental Plants. The Florida Entomologist, Vol. 72, No. 3 (Sep., 1989), pp. 403-407.

Jha, L.K. and Sarma, P.K. 2008. Agroforestry. Indian Perspective. APH Publishing Corporation. New Delhi. 341 p.

Kalshoven, L.G.E. 1981. The Pests of Crops in Indonesia. Revised and translated by P.A. Van deer Laan. PT. Ichtiar Baru-Van Hoeve, Jakarta

Kinota,K. 2006. Common insect in Sapporo (in Japanese). Hokkaido Daigaku Aifud Press. 413 p.

Nishida, E. 1983. Biologies and parasite complexes of two bagworms, *Eumeta japonica* and *Eumeta minuscula* (Lepidoptera: Psychidae) in Japan. Kontyu, Tokyo, 51 (3):394-441

Rhainds, M., Donald Davis, and PeterW. Price. 2009. Bionomics of Bagworms (Lepidoptera: Psychidae). Annu. Rev. Entomol. 2009. 54:209–216.

Sawada, Y. and Arakawa, R. 2002. Field Parasitism of Bagworm, *Eumeta variegata* (Lepidoptera: Psychidae) by the Newly Invaded Parasitic Fly, *Nealsomyia rufella* (Diptera: Tachinidae) in Kochi Prefecture, Japan. Japanese Journal of Entomology New Series Vol.5,No.4, pp, 111-119, (2002)

SURVIVAL OF PATHOGENIC BACTERIA IN YOGHURT AND KEFIR DURING FERMENTATION PROCESS AND COLD STORAGE

E. Taufik[1,3*], R.R.A. Maheswari[1], I. Sudirman[2], Z. Wulandari[1], T. Pratiwi[1], A. Paramita[1] and T. Syaifulina[1]

[1/*]Department of Animal Production Science and Technology, Faculty of Animal Science, Bogor Agricultural University, Indonesia. Jl. Agatis Kampus IPB Darmaga, Bogor INDONESIA 16680
E-mail: s21608@st.obihiro.ac.jp
[2] Department of Animal Disease and Veterinary Public Health, Faculty of Veterinary Medicine, Bogor Agricultural University, Indonesia. Jl. Agatis Kampus IPB Darmaga, Bogor INDONESIA 16680
[3]Graduate School of Animal and Food Hygiene, Obihiro University of Agriculture and Veterinary Medicine. Hokkaido, Obihiro, Inada Cho Nishi 2-11, JAPAN 080-0855

Abstract: Fermentation has been used as primary mechanism in preserving and increasing safety of milk products. Consequently, fermented milk products are generally considered as safe product. The contamination of pathogenic bacteria into the milk may occur in the farm or during handling and processing of the milk products. The contamination source might be originated from the environment, mammary gland, utensils, and workers. Thus, the quality of starter culture which is used in the production of fermented milk play an important role. Therefore the objective of this experiment is to study the antagonistic activity of yoghurt and kefir starter culture on the survival of *Staphylococcus aureus* (SA) KT07 and *Escherichia coli* (EC) KT07 as indicator of pathogenic bacteria during 24 hours of fermentation and 11 days of cold storage (5±2°C). The experiment was done by addition of pathogenic bacteria into the yoghurt (YT), probiotic yoghurt (YP), and kefir (Kf). The starter bacteria that used in this experiment were *Streptococcus thermophilus* (ST) RM01 + *Lactobacillus bulgaricus* (LB) RM01 for YT; ST RM01 + LB RM01 + *Bifidobacterium longum* (BL) RM01 for YP; and bulk starter of *kefir grain* for Kf. The examined variables were pH, titratable acidity, population of lactic acid bacteria (LAB) and pathogenic bacteria. The variables were measured every 4 hours for 24 hours fermentation and every 2 days during cold storage for 11 days. The results showed that the number of lactic acid bacteria (LAB) in the fermented milks with SA KT07 as testing bacteria increased after 4 hours fermentation process until the end of cold storage. Whereas in the fermented milks with EC KT07 as testing bacteria, the population of LAB increased during fermentation but decreased after 24 hours and sharply decreased until the end of cold storage. The viable count of SA KT07 increased by 8.92% for YT; 6.16% for YP, and 26.42% for Kf during fermentation, and continued to increase until the end of cold storage except in YP. Viable count of EC KT07 also increased during fermentation and reduced sharply to 1.90 log cfu/ml for YT and 0.70 log cfu/ml for YP at the end of cold storage. Based on the results of this experiment, it can be concluded that probiotic yoghurt had better bacteriostatic activity toward testing bacteria among treatments. The results moreover showed that fermented milk products may have potential risk to the consumer health if the manufacturing process is not free from bacterial contamination.

Keywords: *antagonistic activity, yoghurt, kefir, survival, Staphylococcus aureus, Escherichia coli*

1. INTRODUCTION

1.1 Background

Various ethiological agents in milkborne diseases has changed dramatically over time. However, more than 90% of all reported cases of dairy related illness continued to be

of bacterial origin, with at least 21 milkborne or potentially milkborne diseases currently being recognized. Pathogens that have been involved in foodborne outbreaks associated with the consumption of milk include *Listeria monocytogenes*, *Salmonella*, *Campylobacter*, *Staphylococcus aureus*, *B. cereus* and *Cl. botulinum*. The presence of these pathogenic bacteria in milk emerged as major public health concerns (Chye *et al.,* 2004).

The consumer demand on milk products such as pasteurized milk and fermented milk products, were constantly increasing. Product diversifications and direct marketing strategy were just example on how the producers try to cope with this situation. Many small scale fermented milk producers were also established and sell their products directly to the consumers. The food safety status of their products is one of the most sensitive issues that should be concerned in terms of consumer's health protection.

1.3 Formulation of the Problem

Due to its intrinsic characteristics such as organic acids contents and the availability of lactic acid bacteria as starter culture, the fermented milk products are considered to be safe to consume. In the other word, it has GRAS (Generally Recognized As Safe) status. The organic acids produced by lactic acid bacteria have the ability to inhibit or kill pathogenic bacteria, but this ability is determined by the quality of starter culture and the contamination degree of the raw material. The problem is then raising, if the raw material is heavily contaminated either from premises in the farm, during the production process such as incompleted fermentation process or contamination from worker or utensils; how far those pathogenic bacteria can survive during the processing and storage? Can we still consider the fermented milk products as safe food? Therefore, the study on the survival of pathogenic bacteria during fermentation process and cold storage is of central importance.

2. OBJECTIVE

To investigate the antagonistic activity of yoghurt and kefir starter culture on the survival of *Staphylococcus aureus* (SA) KT07 (Gram positive) and *Escherichia coli* (EC) KT07 (Gram negative) as indicator of pathogenic bacteria during 24 hours of fermentation and 11 days of cold storage (5±2°C).

3. MATERIALS AND METHODS

3.1 Materials

The starter bacteria that used in this research were *Streptococcus salivarius* subsp. *thermophilus* (ST) RM01, *Lactobacillus delbrueckii* subsp. *bulgaricus* (LB) RM01*,* bulk starter of kefir grain RM01 and *Bifidobacterium longum* (BL) RM01. All bacteria were collection of Division of Dairy Science, Department of Animal Production Science and Technology, Faculty of Animal Science of Bogor Agricultural University. Whereas the pathogen isolates of *Staphylococcus aureus* KT07 and *E.coli* KT07 were isolated from raw goat milk by Taufik (2007). The chemicals that used were MRSA (*de Mann Rogosa Sharpe Agar*), BPA (*Baird Parker Agar*) with *egg yolk tellurite*, E/C Petrifilm, EMBA (*Eosin Methylene Blue Agar*), BHIB (*Brain Heart Infusion Broth*), sterile standard liquid of NaCl, 0.5 McFarland standard, alcohol, buffer solution of pH 4 and 7, PP (*Phenopthalein*) 1%, NaOH 0.1N. Standard microbiological equipments were used to run the sample analysis.

3.2 Methods

3.2.1 Fermented milk

The process of yoghurt making was based on the method explained by Tamime et al, (1999). Two types of yoghurt were produced i.e. yoghurt type I (YT) and type II (YP). Each type contained 5% of culture starter, *L. bulgaricus* (LB) RM01 and *S. Thermophilus* (ST) RM01 were used in type I yoghurt and LB RM01 and ST RM01 plus *Bifidobacterium longum* (BL) RM01 were used in type II yoghurt.

Kefir (Kf) was made by modification of method reported by Gulmez et al, (2003). The starter culture of bulk kefir grain was added in the same concentration with yoghurt starter culture (5%). The indicator pathogenic bacteria in about 10^6 cfu/ml (6 log cfu/ml) were added to each fermented milk type along with the starter bacteria. Incubation was done for 24 hours at 37^{o}C for yoghurt and 28^{o}C for kefir.

3.2.2 Pathogenic Bacteria

The pathogenic bacteria which were used as indicator or testing bacteria represented Gram positive and negative bacteria. *Staphylococcus aureus* (SA) KT07 (Gram positive) and *Escherichia coli* (EC) KT07 (Gram negative) originated from goat milk isolated by Taufik (2007) were used in this experiment.

3.2.3 Sampling Strategy

Fermented milks added with testing bacteria as the treatment i.e. YT+EC/SA, YP+EC/SA and Kf+EC/SA were made as suggested by Estrada *et al.* (2005). Two bottles of sterile milk mixed with each testing pathogenic bacteria were made as positive control (KSA KT07 and KEC KT).

Table 1 Matrix of Treatments, Control and Sampling Time of Analysis

Treatments and Control	**YT+EC/SA**			**YP+EC/SA**			**Kf+EC/SA**			**KEC/KSA**		
Replication	1	2	3	1	2	3	1	2	3	1	2	3
Fermentation (hours)												
0	√	√	√	√	√	√	√	√	√	√	√	√
4	√	√	√	√	√	√	√	√	√	√	√	√
8	√	√	√	√	√	√	√	√	√	√	√	√
12	√	√	√	√	√	√	√	√	√	√	√	√
16	√	√	√	√	√	√	√	√	√	√	√	√
20	√	√	√	√	√	√	√	√	√	√	√	√
24/ Storage Days – 0	√	√	√	√	√	√	√	√	√	√	√	√
3	√	√	√	√	√	√	√	√	√	√	√	√
5	√	√	√	√	√	√	√	√	√	√	√	√
7	√	√	√	√	√	√	√	√	√	√	√	√
9	√	√	√	√	√	√	√	√	√	√	√	√
11	√	√	√	√	√	√	√	√	√	√	√	√

Remarks: √ = time of sampling for analysis

3.2.4 Examined Variables

3.2.4.1 pH Value and titratable acidity were measured according to Nielsen (2003).
3.2.4.2 Microbiological Analysis

a. **Total Lactic Acid Bacteria**
   Method from Djenane *et al.* (2005) was followed for counting total lactic acid bacteria
b. **Total *Staphylococcus aureus* (SA) KT07**
   Surface inoculation method was used to count population of SA KT07, this method was carried out based on ISO 6888-1 (ISO, 1999).
c. **Total *Escherichia coli* (EC) KT07**
   Total population of EC KT07 was counted based on 3M™ Petrifilm™ *E.coli/Coliform Count Plates* method (Petrifim™, 2005).

4. RESULTS AND DISCUSSION

The effect of lactic acid bacteria as starter culture of yoghurt (YT), probiotic yoghurt (YP) and kefir (Kf) on the survival of pathogenic bacteria *Stapylococcus aureus* (SA) KT07 and *Eschericia coli* (EC) KT07, as well as on pH value and titratable acidity (TAT) during 24 hours of fermentation and 11 days of cold storage 5±2°C is discussed in the following subtitles.

4.1 For *Stapylococcus aureus* (SA) KT07

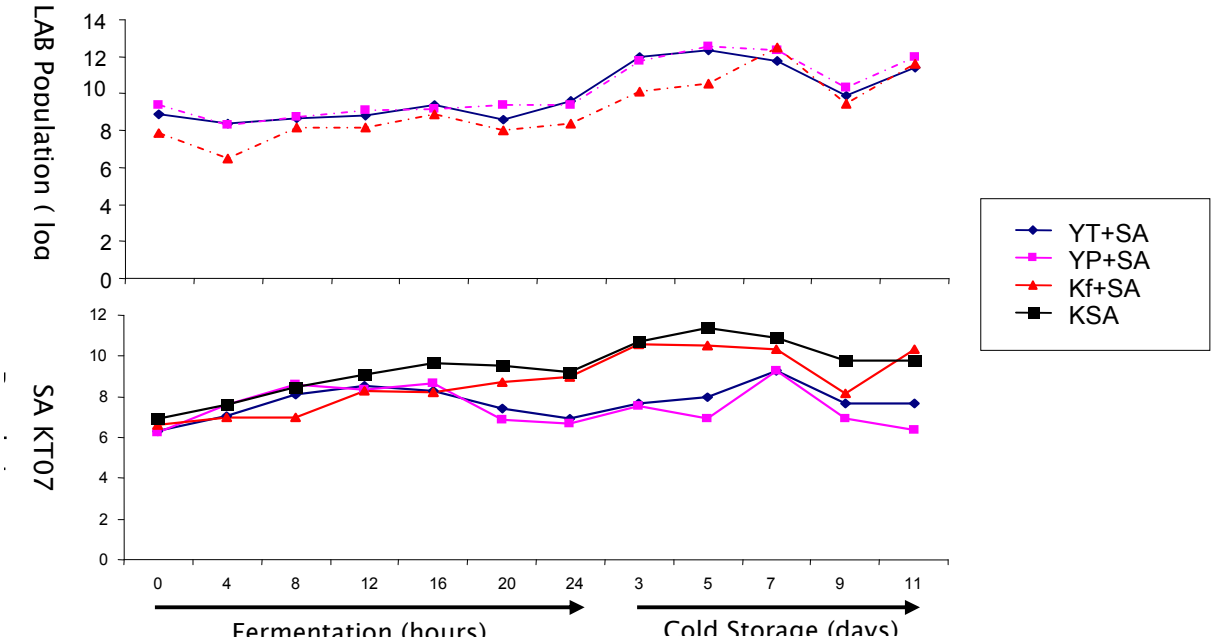

Figure 1 LAB and SA KT07 Population of Each Fermented Milk Product and Control During Fermentation Process and Cold Storage

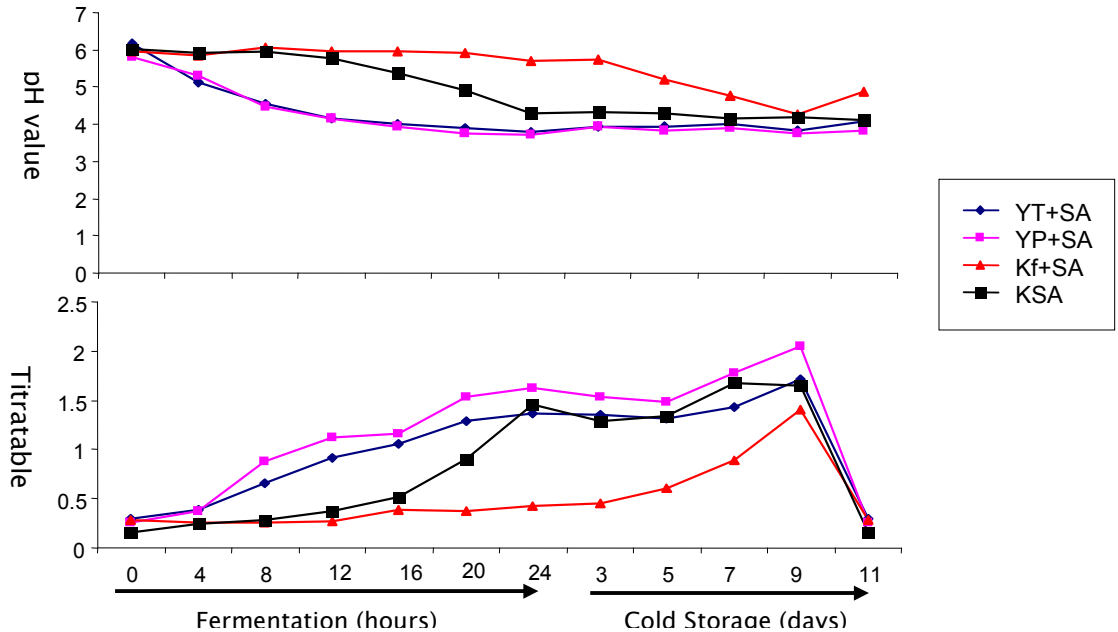

Figure 2 pH and Titratable Acidity (TAT) Value of Each Fermented Milk Product and Control with SA KT07 as The Testing Bacteria During Fermentation Process and Cold Storage

Figure 1 shows that from the beginning of fermentation process until 24 hours (the end of fermentation process), the SA population in all fermented milks were tend to increase. Whilst the population of LAB were tend to be constant though the number of population of LAB was relatively higher than SA. The number of SA population at the end of fermentation in all fermented milks were still remain high (6 – 8 log cfu/ml). Those range of number of SA in the fermented milk posses high risk to the consumer health, since it is still within infective dose. YP had the lowest number of SA at the end of fermentation process among all fermented milks.

The SA and LAB growth pattern in the storage time was relatively similar. The probiotic yoghurt (YP) still had the highest LAB population but lowest pathogenic bacteria (SA) population among other fermented milks. However, the number of pathogenic bacteria (SA) at the end of storage (day 11th) still remain high (above 6 log cfu/ml). The number of SA at the end of cold storage was about in the same number with the beginning of fermentation for YP and higher for other samples. It means that the fermented milk products, either at the end of fermentation process (24 h) as well as after 11 days of cold storage had relatively high risk for consumer health in regard to the pathogenic bacterial load (SA) contained in the products.

pH value for each treatment and control during fermentation process tended to decrease and continued in relatively in constant pattern during storage except for the control (Figure 2). pH value of fermented milk i.e. YT+SA, YP+SA and Kf+SA at the end of fermentation process (24 h) were 3.79; 3.73; and 5.70 respectively. As the pH measure the concentration of H in the solution, the titratable acidity (TA) value showed the degree of acidity. Therefore the value of pH and TA are opposite of each other as it shown in the Figure 2.

The decreasing of pH value was related with the metabolism of lactose into lactic acid and other organic acids by the activity of lactic acid bacteria. Although the pH decreased, the pH value at the end of fermentation process (24 h) as well as at the end of cold storage for YT+SA, YP+SA, KYT and KYP was in accordance with standard pH value for yoghurt according to Jay *et al.* (2005) which is in the range of 3.65 – 4.4.

4.2 For *Eschericia coli* (EC) KT07

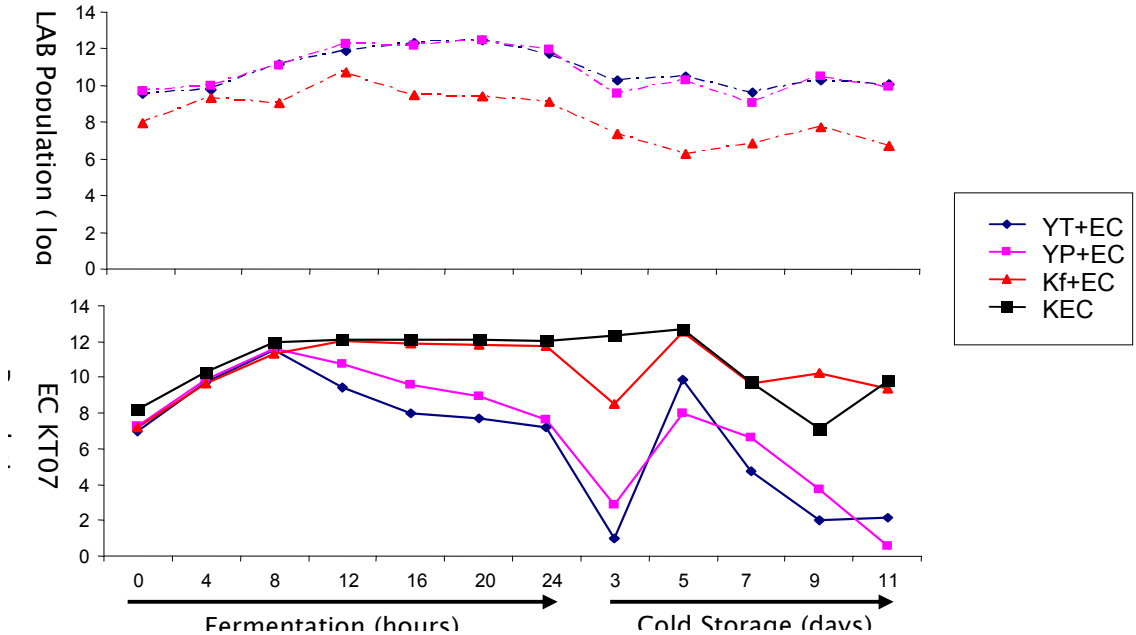

Figure 3 LAB and EC KT07 Population of Each Fermented Milk Product and Control During Fermentation Process and Cold Storage

Population of LAB and EC KT07 of each fermented milk product and control during fermentation process and cold storage is shown in Figure 3. LAB population for YT+EC increased from 9.58 log cfu/ml at starting point of fermentation process (0 h) to 11.74 log cfu/ml at the end of fermentation process (24 h). Population of LAB from YP+EC treatment also increased from 9.72 log cfu/ml at early fermentation (0 h) to 11.95 log cfu/ml at the end of fermentation process (24 h). Whereas the population of LAB for Kf+EC also increased from 7.97 log cfu/ml at early fermentation to 9.10 log cfu/ml at the end of fermentation. In regard to LAB population, YP+EC had higher content of LAB compared to YT+EC treatment. This was due to the number of LAB cells itself, where YP + EC starter had more LAB strain compared to others.

Based on the number of LAB at the end of fermentation process, the yogurt group of treament (YT and YP) had shown best microbiological quality referring to the standard according to Jay *et al*. (2005) which stated that new fresh yoghurt must contain LAB in about 10^9 cfu/g.

LAB population tended to decrease during cold storage, the decrease of LAB population in all treatments from day 0 to day 3 was likely to be associated with the growth phase of bacteria. Within that time period, the growth phase of bacteria has passed the stationary phase and start to enter declining phase. Another factor that affect on the decrease of LAB population was the acid accumulation as the result of fermentation process. The accumulated acid can inhibit the

growth of bacteria as the pH value become decreased (Figure 4). Population of LAB at the end of cold storage for all treatments and control still in accordance with standard of fermented milk. The number of LAB contained in the fermented milk should be at least 10^7colony/ml (Kurmann et al., 1992). The differences among treatments and control on the population of LAB reflected the characteristics of each group of starter bacteria.

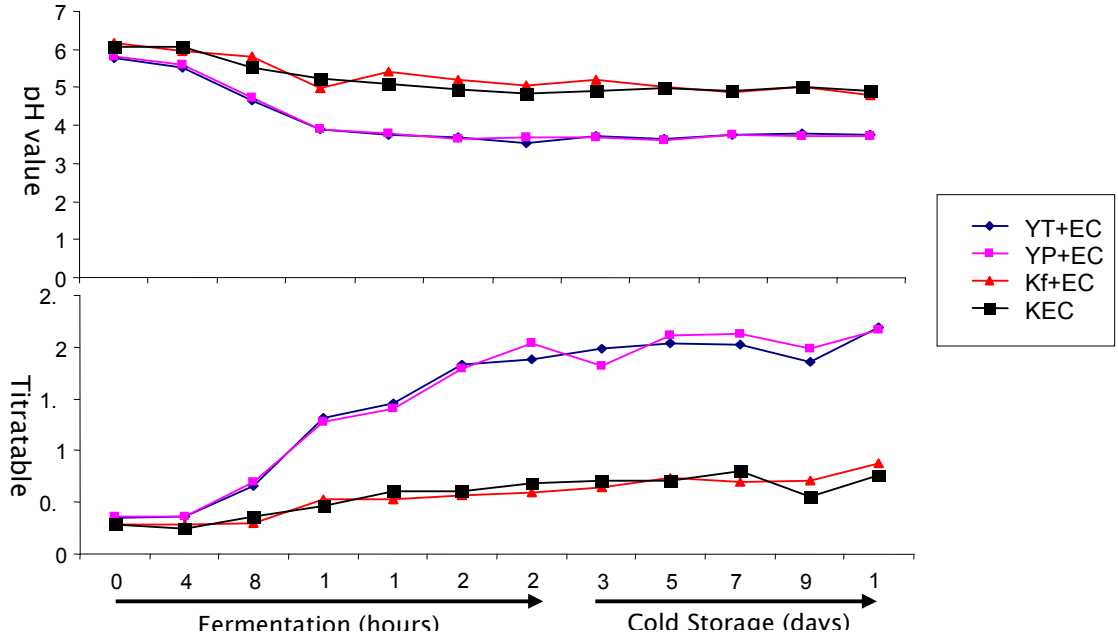

Figure 4 pH and Titratable Acidity (TAT) Value of Each Fermented Milk Product and Control with EC KT07 as The Testing Bacteria During Fermentation Process and Cold Storage

EC KT07 bacteria can survive in all treatments and grew in high number. The high increasing of EC KT07 population showed by Kf+EC, started from 6.95 log cfu/ml at early fermentation grew into 11.49 log cfu/ml at the end of fermentation process (24 h). This increasing of EC KT07 in Kf+EC was likely to be associated with pH and TAT value (Figure 4) which was also affected by LAB activity. The acid production of Kf+EC starter bacteria was very slow resulted in high pH value as compared to other treatments. This condition supported EC KT07 to grow in optimum condition, because the final pH value (5.4) of Kf+EC was above the minimum pH value requirement for EC bacteria to grow. The minimum pH value for EC bacteria to grow is around 4.4 (Blackburn et al., 2003).

5. CONCLUSIONS

1. Probiotic yoghurt had better bacteriostatic/antagonistic activity toward testing bacteria among treatments.
2. High level pre-fermentation contamination of the fermented milk products posses high risk to the consumer health status, either at the end of fermentation or after cold storage.
3. Fermented milk products which are widely recognized as safe product due to its low pH and LAB content will posses potential risk for the consumer's health if the contamination occur during processing and storage.

ACKNOWLEDGEMENTS

We would like to express our gratitude to the management of PHK A2 Program of Department of Animal Production Science and Technology, Faculty of Animal Science, Bogor Agricultural University for granting us the financial support of this study. Sincere gratitude also goes to all technicians and supporting staffs who helped us throughout the study.

REFERENCES

Blackburn, CW, McClure PJ. (2003) Foodborne Pathogens (Hazards, Risk Analysis and Control). Woodhead Publishing Limited, Cambridge, England.

Chye FK, Abdullah A, Ayob MK. (2004) Bacteriological quality and safety of raw milk in Malaysia. Food Microbiol 21: 535-541

Djenane D, Martínez L, Blanco D, Yangüela J, Beltrán JA, Roncalés P. (2005) Effect of lactic acid bacteria on extention of shelf life and growth of *Listeria monocytogenes* in beef steaks stored in CO_2-rich atmosphere. Brazilian J Microbiol 36: 405-412

Estrada AZ, de la Garza LM, Mendoza MS, Lopez EMS, Kerstupp SF, Merino AL. (2005) Survival of *Brucella abortus* in milk fermented with a yoghurt starter culture. Rev Lat Microbiol 47 (3-4): 88-91

Gulmez M, and Guven A. (2003) Survival of *Escherichia coli* 0157:H7, *Listeria monocytogenes* 4b and *Yersinia enterocolitica* 03 in ayran and modified kefir as pre- and postfermentation contaminant. Vet Med - Czech 48 (5): 126-132

[ISO] International Organization for Standardization 6888-1. (1999) International Standard: Microbiology of food and animal feeding stuffs - horizontal method for the enumeration of coagulase-positive staphylococci (Staphylococcus aureus and other species). Part 2: Technique using Baird Parker agar medium. International Organization for Standardization. Geneve.

Jay JM, Loessner MJ, Golden GA. (2005) Modern Food Microbiology. 7th ed. Springer. New York.

Kurmann JA, Rasic JL, Kroger M. (1992) Encyclopedia of Fermented Fresh Milk Products: An International Inventory of Fermented Milk, Cream, Buttermilk, Whey and Related Products. Van Nostrand Reinhold. New York.

Nielsen S.S. (2003) Food Analysis. 3th Ed. Kluwer Academic/Plenum Publisher, New York.

Petrifim™. (2005) E. coli and Coliform Count Plates Interpretation Guide. Microbiology Products. 3M Health Care Limited. USA.

Tamime AY, Robinson RK. (1999) Yogurt Science and Technology. 2nd ed. Woodhead Publishing Limited. England.

Taufik E. (2007) Microbiological investigation of raw goat milk from commercial dairy goat farms in Bogor, Indonesia. [Thesis]. Freie Universitaet Berlin, Germany and Chiang Mai University, Thailand

TEMPERATURE AND SALINITY CONTROL ON ORE MINERAL DEPOSITION: FLUID INCLUSION STUDY

E. T. Yuningsih[1] and H. Matsueda[2]

[1]Graduate School of Science, Resource Geology Group, Hokkaido University Japan
(etintiny@yahoo.com)
[2] Hokkaido University Mueseum, Hokkaido University, Japan

ABSTRACT : Microthermometric study of fluid inclusion was carried out on the samples from the epithermal gold-silver-basemetal mineralization of Arinem vein system located at Western Java Indonesia from different levels, stages and minerals types such as quartz, sphalerite and calcite. The freezing and heating measurements were conducted on primary fluid inclusions trapped in those minerals. The inclusions especially primary ones were large enough to study, aqueous, consisting of two phases (liquid and vapor) at room temperature. Three type of fluid inclusion are recognized such as: two-phase primary – pseudosecondary liquid-rich fluid inclusion; two-phase primary – pseudosecondary vapor-rich fluid inclusion; two-phase secondary fluid inclusion.
The results of primary fluid inclusion measurement in quartz from different levels indicate that homogenization temperatures ranges are 156.9º-325.1°C, whereas the temperature of fluid inclusion from sphalerite and calcite are ranges 152.7º-218.0ºC and 140.4º-217.1ºC, respectively. The salinities of inclusion in quartz, sphalerite and calcite determined by final freezing point measurement are less than 4.34 wt % NaCl equiv.. So far, Raman spectroscopic analyses of CO_2, N_2, H_2S and CH_4 performed on selected fluid inclusions detected no volatile component other than H_2O. Temperature versus depth profiles for fluid inclusions with evidence of boiling indicate that the paleowater table was located about 235m above the present erosion level during deposition of the main-stage quartz.

Keywords*: fluid inclusion, microthermometry, quartz, salinity, temperature*

1. INTRODUCTION

Fluid inclusion is a tiny cavity in mineral, 1 to 100 of micrometers in diameter, containing liquid and/or gas, formed by the entrapment in crystal irregularities of fluid, commonly that from which the rock crystallized. Fluid inclusion has provided much information in the study of ore deposit including in the immediate problems of mineral exploration and also understanding the physical and chemical enviroment of ore deposition. Fluid inclusion is applicable for geothermometry as a result of differential shrinkage of the host mineral and the inclusion fluid on cooling from the temperature of trapping to that of observation (Roedder, 1984).

Hydrothermal ore minerals typically form from high temperature aqueous solutions. The trapped fluid in an inclusion preserves a record of the composition, temperature and pressure of the mineralizing environment. An inclusion often contains two or more phases. If a vapor bubble is present in the inclusion along with a liquid phase, simple heating of the inclusion to the point of resorption of the vapor bubble gives a likely temperature of the original fluid. If minute crystals are present in the inclusion, such as halite, sylvite, hematite or sulfides, they provide direct clues as to the composition of the original fluid.

Microthermometric study was carried out on the samples from the epithermal gold-silver-basemetal mineralization of Arinem vein system located at Western Java Indonesia (Fig. 1). The proposed of this study are to understand the characteristic of the fluid inclusion trapped, and to determine the physical and chemical environments of ore mineral deposition.

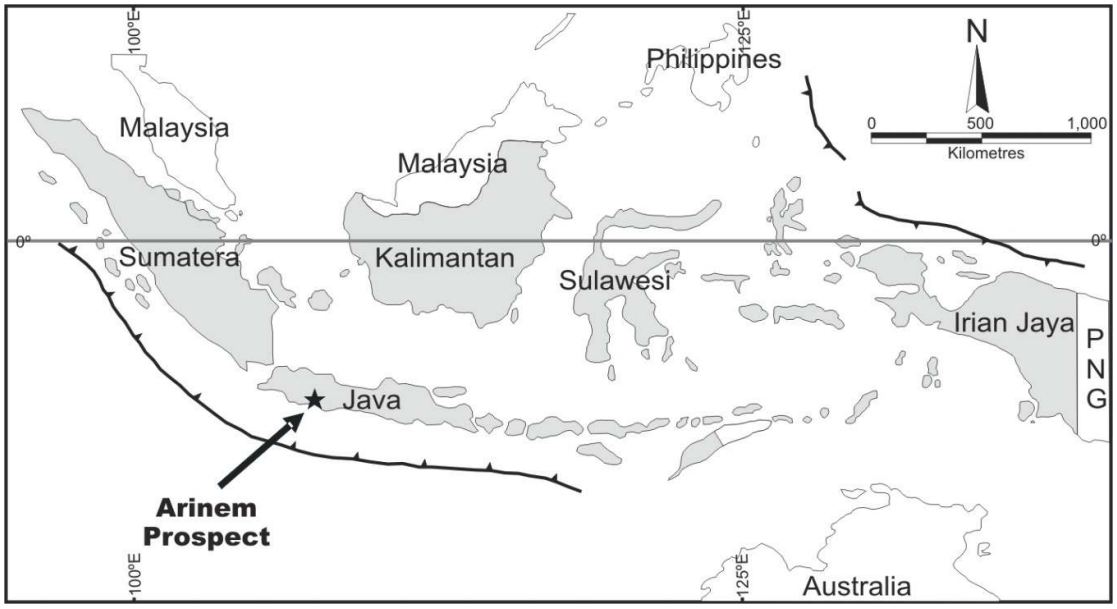

Fig. 1 Map of the Indonesia region indicates the location of the Arinem prospect shows by black arrow.

2. REGIONAL GEOLOGY

The Indonesia archipelago has been formed by three major crustal elements: the Asian Plate, the Indian-Australia Plate and the Pacific Plate. In the tectonic framework distinction is made between West Indonesia and East Indonesia. West Indonesia is situated in the zone of subduction of the Indian-Australian Plate under the Asian Plate. At the surface this junction is expressed by the forming of an island arc, namely the Sunda-Banda arc extending from North Sumatra to the Banda Island (Carlile et al, 1994; Bemmelen, 1949). The plate movement probably started in the Early Creataceous and subduction occurred at least since the Late Cretaceous and at present active subduction is taking place in the south of Java (Clements et al, 2007; Martodjojo, 1982).

The subduction occurred at Late Oligocene to Early-Middle Miocene resulted volcanic and magmatism activities was ended by quartz diorite intrusion at late of Middle Miocene caused of propilitization alteration of Jampang Formation at some places and resulted the important mineralization process (Corbett et al, 1998; Marcoux & Milesi, 1994). Volcanic rock consists of andesitic tuff, tuffaceous breccia and lava with Late Oligocene – Middle Miocene age of

Jampang Formation in the research area is acts as a host for the Arinem mineralization. A quartz diorite intrusion of late Middle Miocene age observed in the prospect area intruding into those volcanic rocks and composed of plagioclase, hornblende, pyroxene with groundmass of fine grained of plagioclase. Tuffaceous breccias, undifferentiated old and

young volcanic groups (Alzwar et. al, 1992) of Tertiary and Quaternary age are widely distributed and cover most of the area.

The Arinem vein system comprises three groups of mineralized quartz veins, named as the Arinem, Bantarhuni and Halimun veins (Antam, 1993). The main vein Arinem is composed mainly of quartz, calcite, sericite and other clay minerals, with variable amount of manganese oxide and limonite and with very rich amount of sulfides. The colorless, white, pale grey, brownish-reddish white, and brownish black fine-coarse grained quartz is observed, due to the content of dominant minerals. Quartz textures of colloform, crustiform, comb, vuggy, massive, brecciated, bladed quartz, and calcedonic are clearly observed and some are presented in Fig. 2.

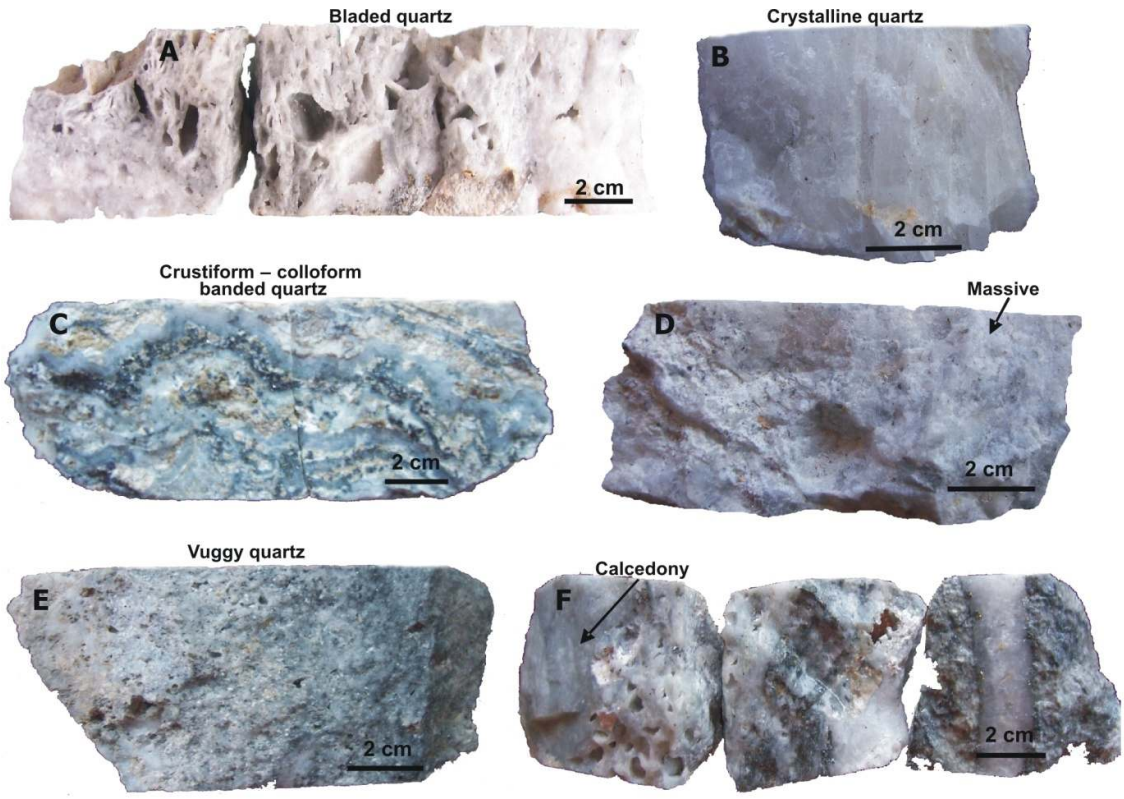

Fig. 2. Hand specimens of Arinem quartz vein from core samples. (A) vuggy and bladed quartz textures of substage IA/L-60m, (B) barren coarse-grained crystalline quartz of substage IIIB/L275m, (C) banding quartz-sulfide of substage IC/L440m, (D) barren massive quartz texture of substage IIIA/L265m, (E) vuggy crystalline quartz of substage IA/L440m, (F) chalcedonic and crystalline barren quartz/substage IIIB cut vuggy crystalline quartz vein of substage IA/L425m.

Based on observation at the L440m (BCAN 3A), L300m (BCBN 2), L265m (BCAN 2A) and L200m (BCBN 3) drill cores of the main vein Arinem, it shows that vein filled reflects three temporal mineralizing stages (I, II and III). Those three distinct stages (vein-forming events) of hypogen mineralization are determined on the basis of structure and mineral paragenesis followed by a supergene stage. Mineralogical observation resulted a three-stage paragenetic sequence of mineralization is proposed based on reflected and transmitted light microscope and electron microprobe studies of 172 polished and double polished thin sections, together with crosscutting relationships between minerals and secondary structural studies.

3. MATERIALS AND METHODS

This study is based mainly on samples collected from exploration drill holes (drilled by PT. Antam Tbk.). These drill holes provide samples at intervals over a strike length of up to 2000m and depth extend of 575m and thus present an opportunity to investigate. Fluid inclusions examined came from four different levels (L440m, L300m, L265m and L200m) in order to document the ranges of fluid compositions and temperatures during the three stages of mineralization and to investigate their variations in time and space. The horizontal extent of sample localities is more than 1km and the vertical interval is approximately 240m.

Double polished plates were prepared on 200μm thickness, apart of quartz at stage III most of the quartz samples were selected for their basemetal sulfide content with the aim of studying fluid inclusions that were associated with deposition of sulfides ± gold and silver. Microthermometric analysis was performed on a Linkam THMSG 600 system attached to a Nikon transmitted-light microscope.

Heating rates was maintained near 2°C/min for measurement of homogenization temperature (T_h) and 0.5°C/min for measurement of ice melting temperature (T_m). Precision is calculate as ±0.1°C in the temperature range of the observed phase changes. Accuracy between −60 and −10°C is estimated in the order of ±0.2°C, whereas between −10 and +30°C and above +200°C is placed at ±0.5 and ±2°C, respectively. Instrumental calibration was done using synthetic pure H_2O (0°C), Dodecamethylene glycol (82.0°C), Benzanilide (163.0°C), Sodium nitrate (306.8°C), n-tridecane (-5.5°C), n-dodecane (-9.6°C), chlorobezene (-45.6°C), and chloroform (-63.4°C) inclusion standards. Salinity estimates were determined from the final melting temperatures of ice, utilizing the equation proposed by Bodnar (1993).

4. RESULTS

Fluid inclusions (595 primary inclusions) were examined in 13 samples (11 quartz, 1 sphalerite, and 1 calcite). The fluid inclusion data came from medium-coarse grained quartz associated with sulphide and this quartz is referred to as main-stage quartz. Sphalerite is mainly dark – pale colour and crowded with chalcopyrite inclusion and primary fluid inclusions were analyzed in only one sample (BCAN 2A-15/L265m) of stage II mineralization. Fluid inclusion obtained from calcite came from stage III, respectively.

Three types of fluid inclusion are recognized: two-phase primary – pseudo-secondary liquid-rich fluid inclusion; two-phase primary – pseudo-secondary vapor-rich fluid inclusion and two-phase secondary fluid inclusion. The inclusions were considered primary or pseudo-secondary, as they were formed isolated within the crystals, in planar arrays outlining growth

zones, or in healed fractures that terminated against growth zones (Fig. 3). Inclusions in quartz and sphalerite that occur in planes of healed fractures that do not terminate against growth zones were considered secondary; commonly these fractures cut across grain boundaries. Secondary fluid inclusions, <20 μm in length, occur along healed fractures that cut across grain boundaries. whereas pseudo-secondary fluid inclusions, which are less abundant than primary or secondary inclusions, formed only along healed fractures within grains.

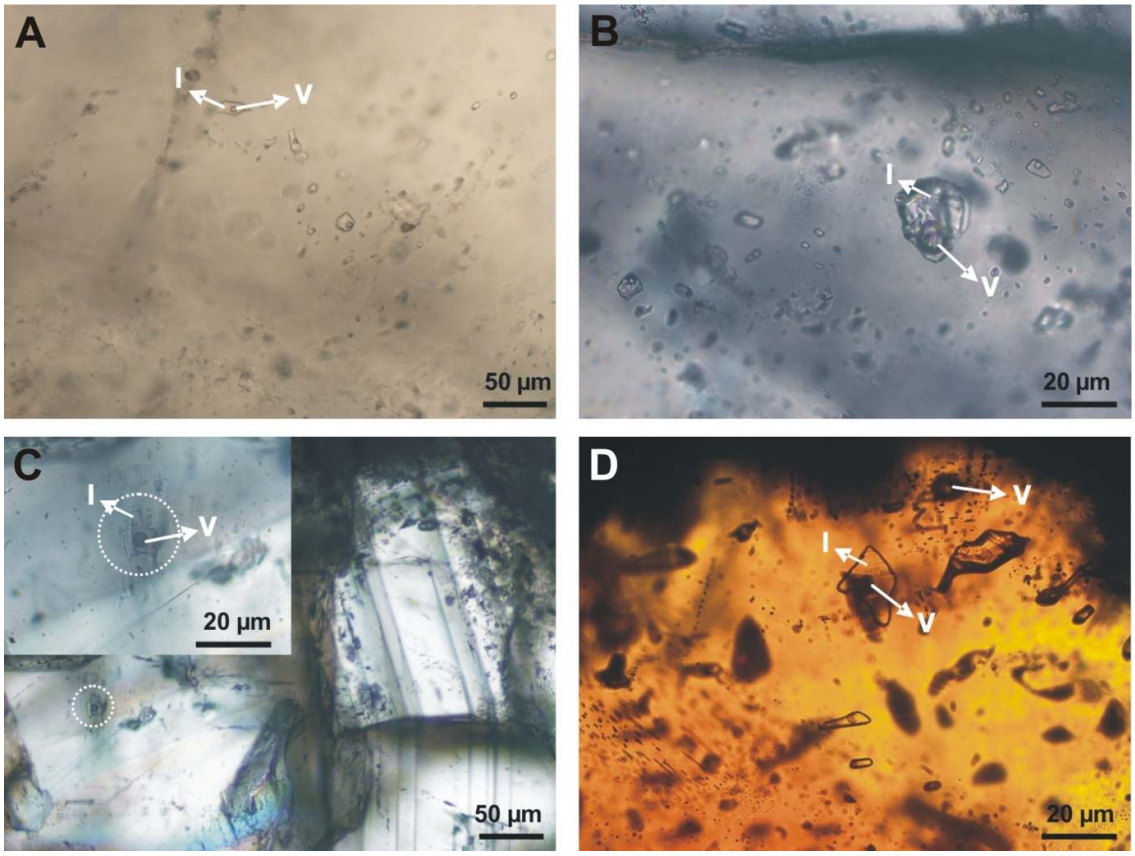

Fig. 3. Photomicrograph of fluid inclusions trapped in quartz, calcite and sphalerite, samples from L265m and L440m of the Arinem quartz vein. (A) group of two phase liquid-rich fluid inclusion as cluster and distributed along the trail in coarse-grain quartz with variable vapor-liquid ratios/substage IIA/L440m, (B) isolated liquid-rich primary fluid inclusion in quartz/substage IB//L265m, (C) isolated two phase liquid-rich primary fluid inclusion trapped in calcite/substage IIIB/L265m, (D) two phase liquid-rich primary fluid inclusion coexists with vapor-rich fluid inclusion trapped in sphalerite /substage IIA/L265m.

According to the criteria of Roedder (1984), the heating and freezing measurements were conducted on primary fluid inclusions trapped in quartz, sphalerite and calcite. The primary inclusion was large enough to study, aqueous, mostly consisting of two phases (liquid and vapor) at room temperature. Type L-V inclusions being dominant in most inclusions (avg >70 vol. %). However, the vapor bubble occupies up to ~90 vol. % of some inclusions. L-V inclusions occur in clear, smoky, and milky quartz, in medium- and coarse-grained calcite, and in substage IIA of sphalerite. Although some of the fluid inclusions were necked down, the ones used in the microthermometric study ranged from 5 to 40µm in length and were classified according to the nomenclature of Roedder (1984).

In this study only primary fluid inclusions and those inclusions which homogenized into the liquid phase were measured. Microthermometric measurements were performed on as many samples as possible, chosen at random, but fewer ice-melting data were obtained than homogenization data due to the small size of the some inclusions. The results of measurements from primary fluid inclusions in quartz for different levels indicate that homogenization temperatures at first stage (I) is in range of 176.6-325.1ºC, second stage (II) 156.9-311.8ºC and last stage (III) is 165.1-236.1ºC. Measurement from sphalerite and calcite

from substage IIA and IIIB give a result of 152.7-218.0ºC and 140.4-217.1ºC, respectively (Table 1). However, quartz sample from L200m of stage I mineralization shows evidence of boiling since this sample contains both gas-rich and liquid-rich inclusions along the same growth band. The filling temperatures of these two types of inclusions range from 216.8-247.3ºC. These data were interpreted to indicate that actual boiling took place at 216.8ºC whereas higher filling temperatures resulting from the trapping of various liquid : vapor proportions.

Ice melting temperatures range from -2.6 to (-0.1)ºC, with distribution of apparent salinity in all stages and level of mineralization vein body. During freezing of inclusion measurement, no unusual solid phase such as CO_2 hydrate was observed in all samples. Fluid inclusion assemblages from main stages I and II from all level, commonly show a narrow range in Tm values (0.18 to 4.34 wt % NaCl equiv.). This is also marked in fluid inclusion assemblages from late stage (stage III) of barren quartz. The salinity determined from quartz is in average 1.95 wt% NaCl equiv., 2.64 wt% NaCl equiv from sphalerite and 2.1 wt% NaCl from calcite, respectively (Table 1).

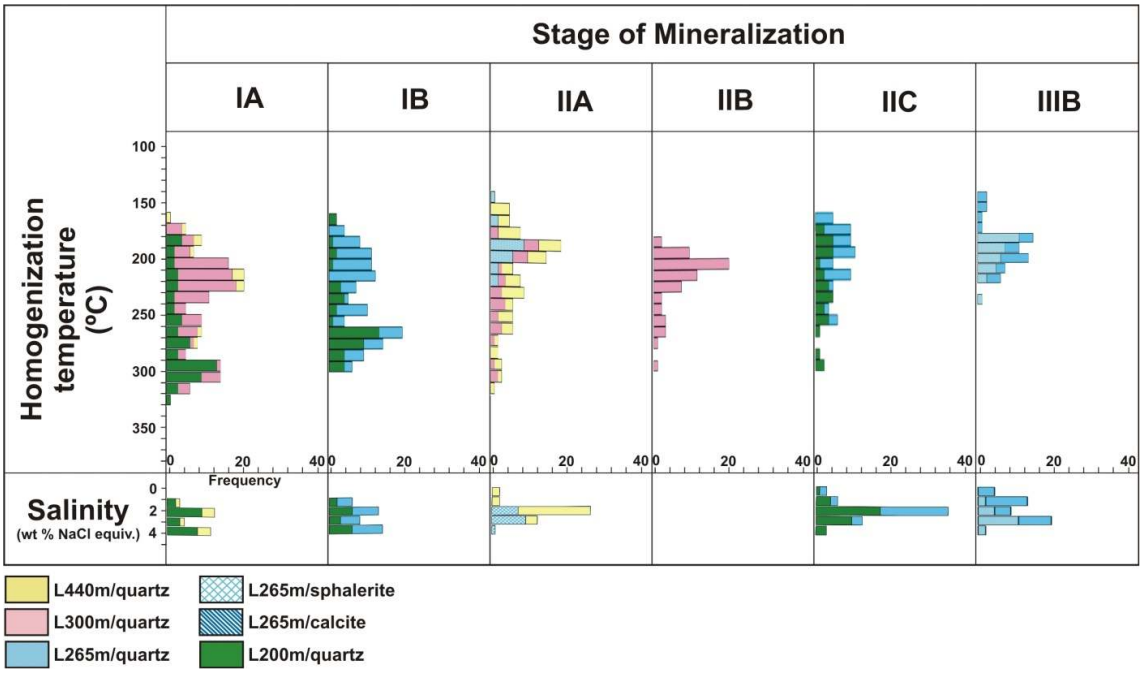

Table 1 Range of fluid inclusion homogenization temperatures and salinity every stage of Arinem vein mineralization

Raman spectroscopic analyses of CO_2, N_2, H_2S and CH_4, performed on selected fluid inclusions detected no volatile component other than H_2O. Temperature versus depth profiles for fluid inclusions with evidence of boiling indicate that the paleowater table was located about 235m above the present erosion level during deposition of the main-stage quartz (Fig. 4). In order to estimate the true temperature of mineralization from filling temperatures of fluid inclusions, the pressure on the fluid must be known. No pressure correction is needed for inclusions trapped while the fluids were boiling. The presence of vapor-rich inclusions in the sample indicates that P-T conditions probably were close to the liquid-vapor, two-phase (boiling) curve. This conclusion is supported by the present of bladed texture of quartz after calcite in some samples. From the temperature-pressure-salinity data on salt solutions

summarized by Hass (1971) it was obtained a fluid pressure of 21.7 bars with an average fluid density of 0.861 g/cm^3 of 2 wt % NaCl equiv. fluid at 216.8ºC.

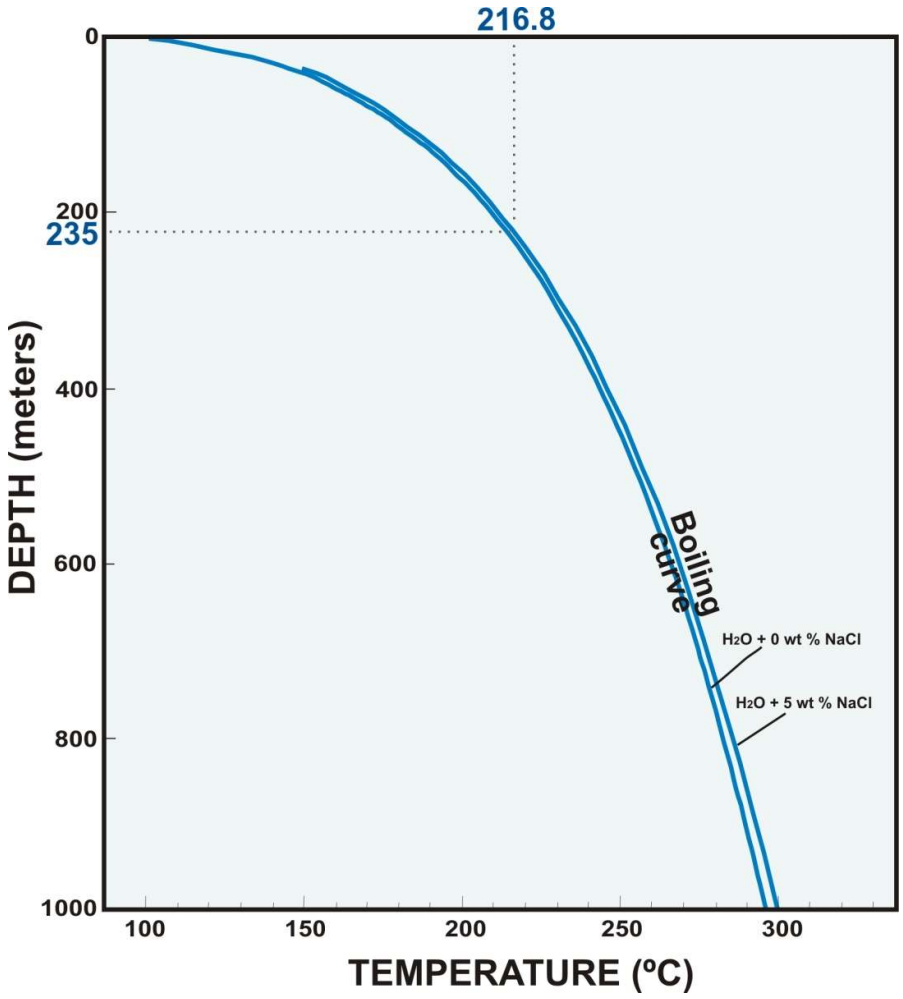

Fig. 4 Possible boiling point with depth curves for water with 0 and 5 wt % NaCl equiv. (Hass, 1971). dashed line showing evidence for trapping of a boiling fluid occurred in substage IA of Arinem vein.

5. CONCLUSIONS

Preliminary fluid inclusion study for the mineralization at Arinem vein system suggest that fluids responsible for this mineralization was formed from fluids with broadly characteristics low-moderate temperature range between 156.9º-325.1°C (with average 194.0º to 267.3ºC), slightly low salinity (up to 4.34 wt % NaCl equiv., in average around 2 wt % NaCL equiv.). Although it has not been demonstrated that these were the fluids which also precipitated the precious metals in these deposits, such fluids are very similar to those advocated for numerous precious and basemetal vein deposits associated with shallow, calc-alkaline, igneous rocks (Roedder, 1984, Hayba et al, 1985).

ACKNOWLEDGEMENTS

The first author wish to thank Antam Tbk for support to access to data and samples during the field investigation and to acknowledge the contribution of the large member of geologic staff who have worked on the Papandayan exploration program.

REFERENCES

Alzwar, M., Akbar, N., Bachri, S. (1992) Systematic geological map, Indonesia, quadrangle Garut 1208-6 & Pameungpeuk 1208-3, scale 1 : 100.000. Geological research and development centre., 1 sheet.

Bodnar, R. J. (1993) Revised equation and table for determining the freezing-point depression of H_2O-NaCl solution. Geochimica et Cosmochimica Acta., vol.57, p683-684.

Carlile, J. C. and Mitchell, A. H. G. (1994) Magmatic arcs and associated gold and copper mineralization in Indonesia. Geochemical Exploration., vol.50, p91-142.

Clement, B and Hall R. (2007) Creataceous to Late Miocene Stratigraphic and Tectonic Evolution of West Java. Indonesia Petroleum Association., 31st Annual Convention and Exhibition, IPA07-G-037.

Corbett, G J. and Leach, T M. (1998) Southwest Pacific Rim gold-copper systems: structure, alteration, and mineralization. Society of Economic Geologists., Special Publication, vol.6, p69-82.

Antam (1993) Gold-silver deposit exploration report DMP, Mt. Papandayan area, Garut regency, West Java province (KP.DDU. 866/Jabar). Unpubl. report (in Indonesian)., 68p.

Haas, J. L. (1971) The effect of salinity on the maximum thermal gradient of a hydrothermal system at hydrostatic pressure. Economic Geology., vol.66, p940-946.

Marcoux, E. and Milesi, J. P. (1994) Epithermal gold deposit in West Java, Indonesia: Geology, age and crustal source. Geochemical Exploration., vol.50, p393-408.

Martodjojo, S. (1982) Evolution of Bogor Basin, West Java. Unpubl. PhD thesis ITB., 412p.

Roedder, E. (1984) Fluid Inclusions: Reviews in Mineralogy. Mineralogical Society of America., vol.12, 644p.

Van Bemmelen, R. W. (1949) The geology of Indonesia. Government printing office., The Hague, Netherlands, vol. IA.

NUMERICAL SIMULATION OF THE 1883 KRAKATAU TSUNAMI PROPAGATION

Aditya Riadi Gusman[1,2], Hamzah Latief[2], and Haris Sunendar[2]

[1]Institute of Seismology and Volcanology, Hokkaido University, Kita 10 Nishi 8 Kita-ku, Sapporo, Japan
E-mail: adit@mail.sci.hokudai.ac.jp
[2]Department of Oceanography, Bandung Institute of Technology, Ganesha 10 Bandung, Indonesia

ABSTRACT: Tsunamis that were generated by the eruption of Krakatau volcano August 27, 1883 devastated the coastal area around Sunda Strait. This study assumed the collapsing Krakatau caldera as the generating force for tsunami numerical simulation.We simulated source models of the tsunami based on the estimated dimension of the collapsed caldera. The source model that used bathymetry data to estimate the collapsed caldera can explain well the observed tsunami run-up. Whereas the source model of a cylinder shaped caldera can explain well the observed tsunami arrival time. The caldera models are able to give good explanations of the tsunami arrival time and tsunami run-up.

1. INTRODUCTION

Indonesia is among countries that located near the subduction zones. The Indo-Australia plate is subducting beneath the Sunda plate, the boundary between these plates called the Sunda trench stretches from the Andaman Islands to the north-west until Sumba Island to the east. Great earthquakes in Indonesia are ruptured on the Sunda subduction zone and most of these earthquakes generated large tsunamis. From 106 tsunami events, 90% were generated by earthquakes, 9% were generated by volcanic eruptions, and 1% was generated by landslides (Latief et al., 2000). Tsunami that flooded a coastal area can reach a location from few hundreds of meters to kilometers from shoreline. The ground level at the inundation boundary of a tsunami called the run-up can reach up to tens of meters from sea level.

Among the tsunamis that were generated by volcanic eruptions in Indonesia, the tsunami generated by the 1883 Krakatau eruption has beenwell recordedbyhistory. The Krakatau volcano has a long record of volcanic activities. The first recorded Krakatau eruption in history was in 416 AD that destroyed the Krakatau and forming a 7 km wide caldera, the eruption also left volcano remnants of Panjang Island and Sertung Island. Before the 1883 eruption, the Krakatau Island was formed by three volcanoes which are Rakata, Danan and Perbuatan, in this article we will call these volcanoes or the island as Krakatau volcano. The boundaries of the calderas formed by the 1883 and pre-1883 eruptions are shown in Figure 1. Geographically, the position of the Krakatau volcano is at 6°06'5.8" S and 105°25'22.3" E. Series of eruptions on 26-27 December 1883 destroyed the Danan and Perbuatan volcanoes, and left only half of the Rakata volcano. The catastrophic 1883 eruption was among the largest eruptions in recorded history. The eruption of Krakatau in 1883 was not only felt by the population residing in the vicinity of the Sunda Strait. The amount of energy released and the material thrown affected the earth's atmosphere globally. Decker and Hadikusumo (1961) estimated that the material ejected by the eruption was about 18 km^3. Hendervari (1979) estimated that the energy required to eject the material is equivalent to 1,810 x 10^{26} J. On 29 December 1927 a submarine eruption was observed within the vicinity of Krakatau Islands, a few days later a volcano immerged above the sea surface, this volcano named Anak Krakatau.

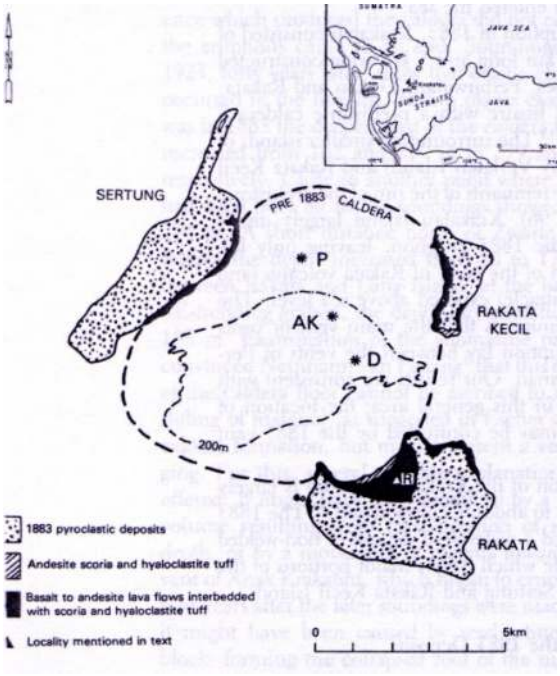

Fig. 1 Boundary of the collapsed caldera (Simkinand Fiske, 1983)

The tsunami generated due to the Krakatau eruption destroyed around 167 villages along the coast of Southern Sumatra and Western Java and killed over 36.000 people. The highest run-up of 41 m was measured in Merak on Java Island. In Betung Bay, Sumatra Island the tsunami dragged a steam ship up to 2.5 km inland along Kuripan River (Simkin and Fiske, 1983). At Anyer 4th Point, a lighthouse destroyed during tsunami inundation,a distribution of coral boulders near the lighthouse suggest that it was destroyed by one of the coral boulders that were transported by the tsunami.

Previous numerical simulation studies of the Krakatau tsunami has been performed by Nakamura (1984), Kawamanta et al., (1992), and Nomanbhoy and Satake (1995). Nakamura (1984) simulated the tsunami using caldera formed by the eruption as the tsunami source. Nomanbhoy and Satake (1995) concluded that the submarine explosion model as the source of the largest tsunami.

In this study we simulated the tsunami propagation generated by the collapsing of Krakatau caldera due to the primary eruption at around 10.00 AM on 27 December 1883. First we simulate the tsunami source using different caldera models, and then we use the source models as the initial sea surface for tsunami simulation. Specifically, we simulate the tsunami run-up and tsunami arrival time at locations where the tsunami was observed. Wethen compare the tsunami simulation results with the observed ones to select which caldera model can best explain the observation.

2. MODELING DOMAIN AND MODELING SETUP

2.1. Modeling Domain

The modelling domainof the tsunami simulation has boundaries of 5°4’ - 6°54’ S and 104°20’-107° E (Figure 2). The bathymetry data is obtainedby digitizing a Bathymetry Map of Dinas Hidro Oseanografi TNI AL, which was printed in 1987.The modeling domain of the propagation model has a size 500 grids × 343 grids in –x and –y directions, respectively, with grid size of 594 m (*d*x = *d*y).

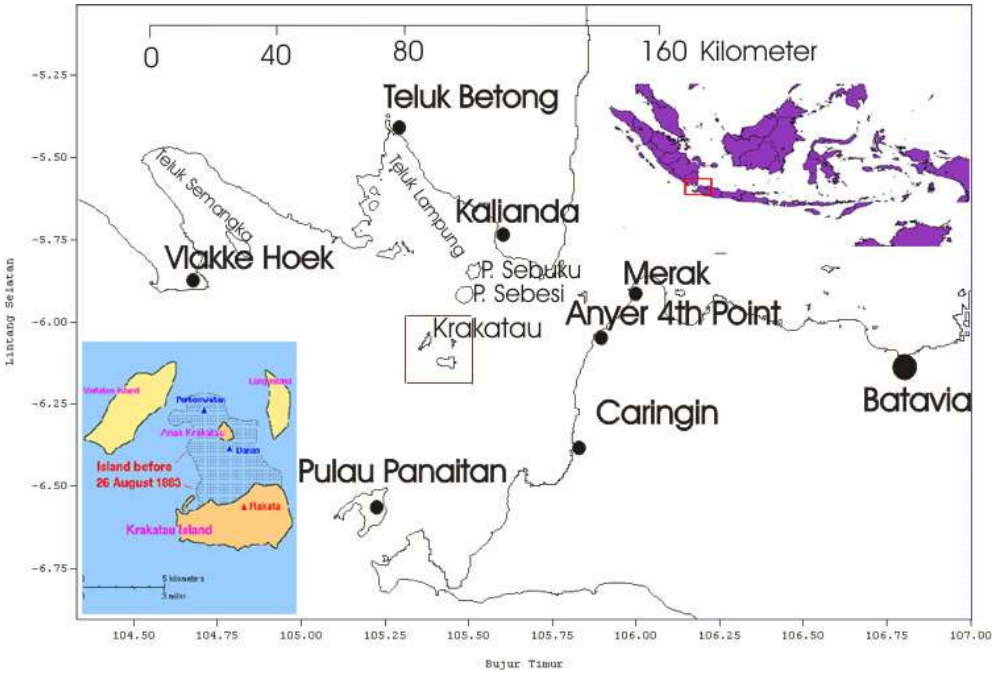

Fig. 2 Map of Sunda Strait
Black dots are location where the Krakatau tsunami was observed. Inset: Map of Indonesia and Krakatau Islands before and after the eruption of 1883 (Simkinand Fiske, 1983)

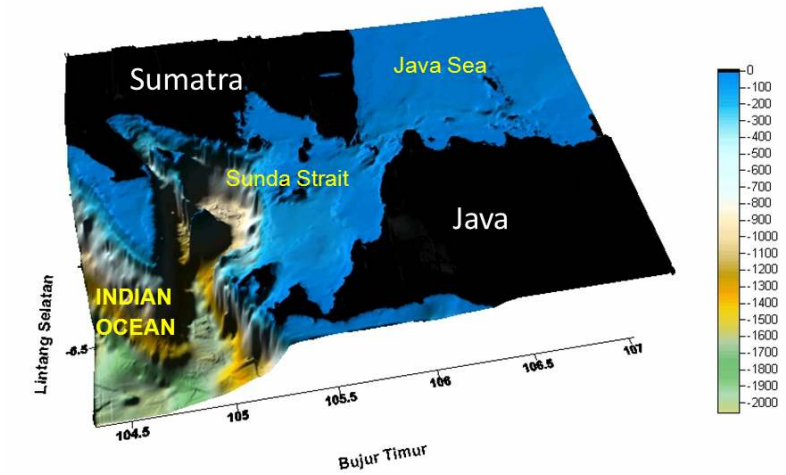

Fig. 3 Bathymetry of Sunda Strait (color bar is in meter)

Krakatau volcano is located in the middle of the Sunda Strait between Java Island to the east side and Sumatera Island to the northwest side. The northeast part of the strait is narrowing before enters the Java Sea. In the southwest side, the strait gets wider and deeper before crossing with continental shelf of Indian Ocean where the depths are change dramatically from 50 m to about 1000 m (Figure 3).

2.2. Krakatau Caldera

For the tsunami source models, we assumed the Krakatau caldera was the main source that generates tsunami along west coast of Java and south coast of Sumatra. In this study we have threescenarios oftsunami simulation with different shapes of caldera models. The caldera models are based on the volume of the Krakatau caldera which was collapsed to the bottom of the sea during the primary eruption. The volume of the Krakatau caldera was obtained by comparing the bathymetry around Krakatau before and after the eruption. The bathymetry data around Krakatau volcanobefore the eruption was produced by the British Admiralty Charts, 4th edition of the year 1868 (Figure 4). The bathymetry data around the Krakatau caldera after the eruption (Figure 5) was produced from a survey in 1885 by Verbeek. Fromthose bathymetry data the volume of collapsed caldera is calculated to be about 8.6 km^3.

Fig. 4 Bathymetry data before the 1883 eruption (*British Admiralty Charts*, 1868).

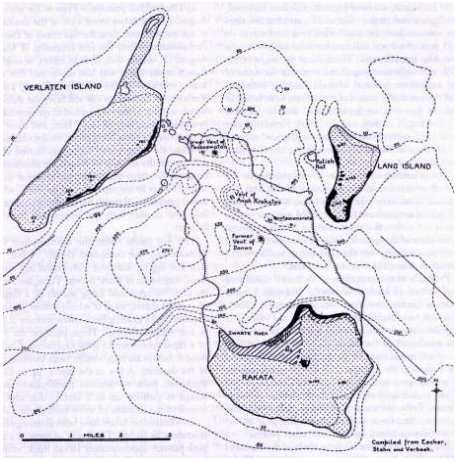

Fig. 5 Bathymetry data after the 1883 Krakatau eruption (Verbeek, 1885)

2.2.1. Scenario I

In this scenario, we approximate the collapsed caldera with a square surface and an average depth of the Krakatau calderawhich was formed after the primary eruption. We approximate that the square sizes 10 × 10 grids with grid size of 594 m. We assumed the sea surface drops instantly to the depth of 200 m (Δt =0). This dimension calculates the volume of caldera model in scenario I as about 7.6 km^3. The modeling area for the source generation has a size of 30 grids in –x direction and 30 grids in –y direction. The tsunami source is simulatedusinga time interval of 0.5 sec (Δt = 0.5 sec).

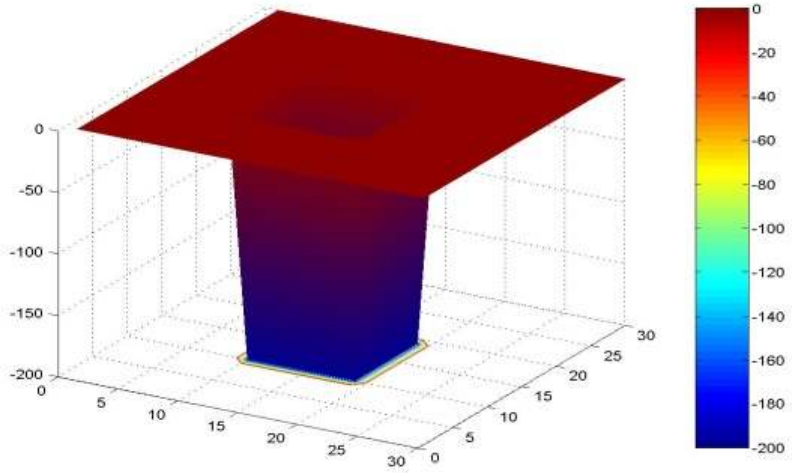

Fig. 6 Model of Krakatau caldera in Scenario I, x and y axes are in grid unit, z axis and color bar are in meter

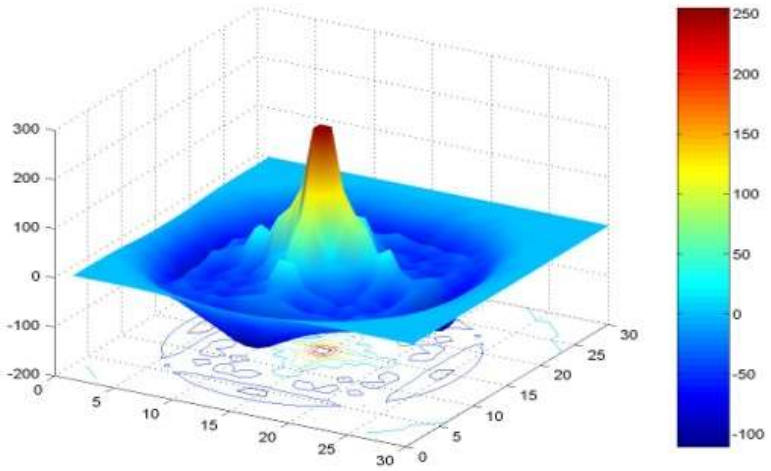

Fig. 7 Initial elevation of the tsunami source in scenario I, x and y axes are in grid unit, z axis and color bar are in meter

2.2.2. Scenario II

In this scenario, we approximate the collapsed caldera with a cylinder shaped caldera. We assumed the sea surface drops instantly to the depth of 200 m ($\Delta t = 0$). The volume of caldera model in scenario II is about 8.6 km^3. The modeling area for the tsunami source generation has a size of 40 grids in –x direction and 40 grids in –y direction. The tsunami source is simulatedusinga time interval of 0.5 sec ($\Delta t = 0.5$ sec).

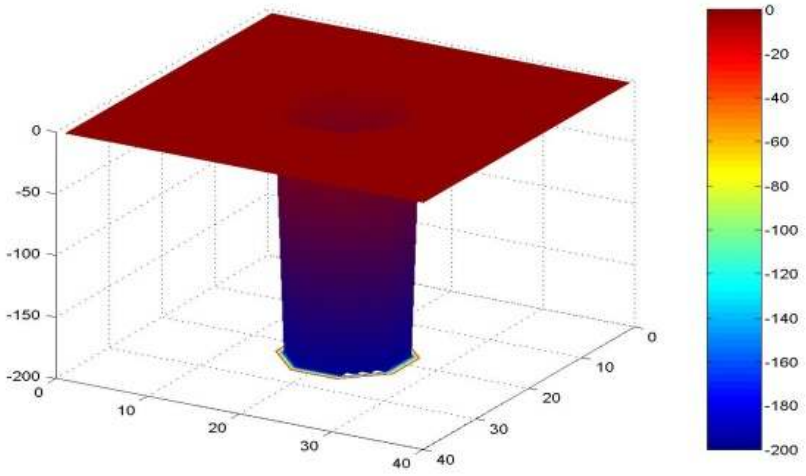

Fig. 8 Model of Krakatau caldera in Scenario II, x and y axes are in grid unit, z axis and color bar are in meter

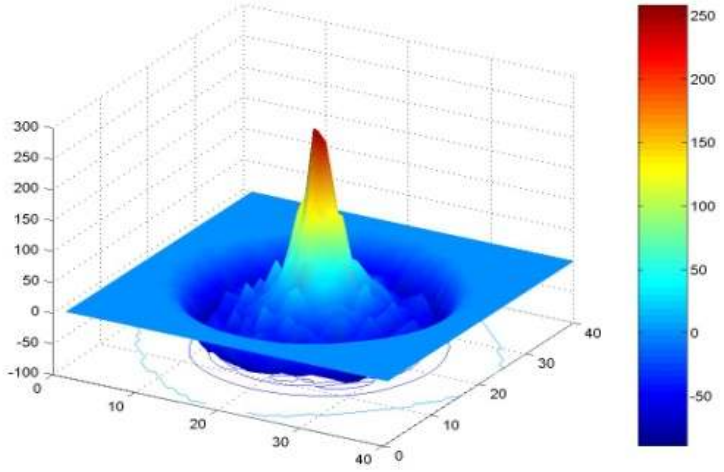

Fig. 9 Initial elevation of the tsunami source in scenario II, x and y axes are in grid unit, z axis and color bar are in meter

2.2.3. Scenario III

In this scenario, we approximate the size of the Krakatau caldera with a more realistic shape obtained using the bathymetry data around Krakatau. The Krakatau caldera model has a volume of 8.6 km^3. The modeling domain of the tsunami source generation has a dimension of 400 × 400 grids in –x and –y directions, where each grid has a size of 54.9 m ($dx = dy$). The tsunami source is simulatedusing a time interval of 0.5 sec ($\Delta t = 0.5$ sec).

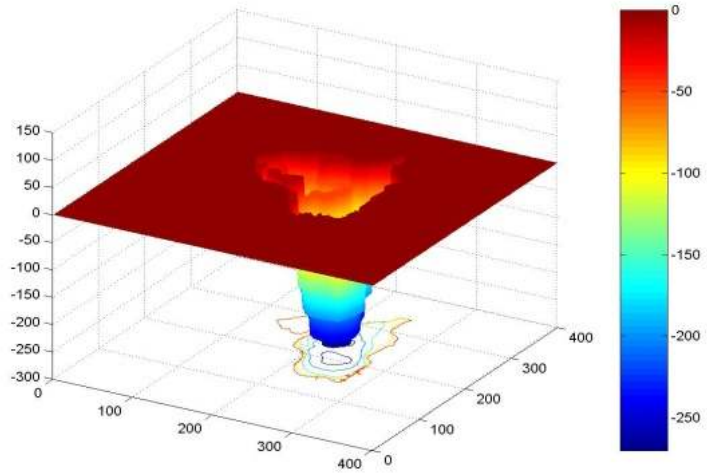

Fig. 10 Model of Krakatau caldera in Scenario III, x and y axes are in grid unit, z axis and color bar are in meter

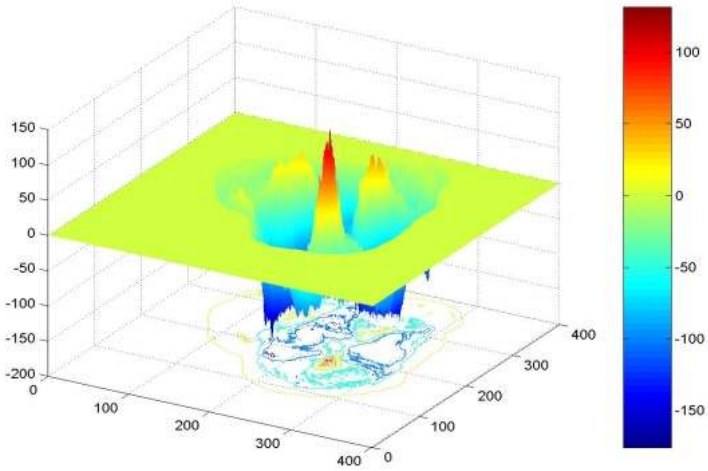

Fig. 11 Initial elevation of the tsunami source in scenario III, x and y axes are in grid unit, z axis and color bar are in meter

2.3. Tsunami Simulation

To simulate the tsunami propagation we solve the linear shallow water equation numerically using the finite different scheme. The governing equations for the tsunami computation explained by Johnson (1999) are the following

$$\frac{\partial h}{\partial t} + \frac{\partial M}{\partial x} + \frac{\partial N}{\partial y} = 0 \quad (1)$$

$$\frac{\partial M}{\partial t} + gD\frac{\partial h}{\partial x} = 0 \quad (2)$$

$$\frac{\partial N}{\partial t} + gD\frac{\partial h}{\partial y} = 0 \quad (3)$$

In the equations, M and N are discharge flux in –x and –y directions, respectively, g is the gravitational acceleration, h is wave height, and D is total water depth (h+d). The above equations are the expression of the linear shallow water theory in Cartesian coordinate system for near field tsunami.

A time interval of 0.5 sec ($\Delta t = 0.5$ sec) is used for tsunami simulation to satisfy the stability condition. The total simulation time is 21600 iterations or 3 hours. The three source models are used for the simulation of tsunami run-up and arrival time at locations indicated by Figure 2.Then we compare the observed tsunami with the simulated ones at these locations to evaluate which scenario can best explain the observations.

3. RESULTS AND ANALYSIS

3.1. Tsunami Run-up

We used observed tsunami run-up in Betung Bay, Kalianda, VlakkeHoek lighthouse, Merak, Panaitan Island, and Anyer 4thPoint. We also used the observed tsunami waveform at Batavia. Tsunami simulation result shows that tsunami propagates with higher speed toward the Indian Ocean and slower speed on the Sunda Strait where the sea is relatively shallower (Fig. 12). The simulated tsunami run-up using the three caldera models and the observed ones are shown in Table 1. The comparison shows that the simulated tsunami run-up from scenario III generally wellexplained the observed tsunami. The other caldera models are not as good as the realistic caldera used in scenario III. However, from the results of three caldera models we could not explain the 41 m tsunami run-up observed in Merak. This may be caused by the grid size that we used being too coarse to model the tsunami in Merak. Local bathymetry and topography around Merak might also play a significant role in generating a high tsunami run-up.

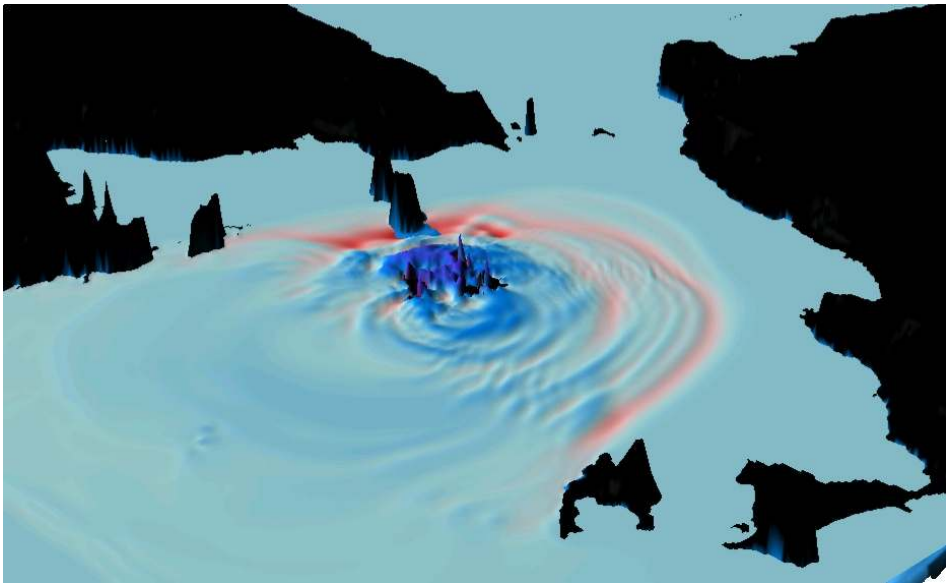

Fig. 12 Snapshot of the simulated tsunami propagation at t = 20 minutes
Red indicate negative elevation and blue indicate positive elevation

Tabel 1. Maximum tsunami run-up

Locations	Simulated tsunami run-up			Observed Tsunami Run-up
	Scenario I	Scenario II	Scenario III	
Betung Bay	29 m	16.5 m	24.3 m	21.9 m
Kalianda	33 m	36.5 m	36 m	24.4 m
VlakkeHoek lighthouse	15.6 m	17.5 m	12.2 m	15.2 m
Merak	15.6 m	27 m	21.8 m	15 - 41 m
Panaitan Island	21.2 m	40 m	16.6 m	15.2 m
Caringin	23.8 - 30 m	41 m	19.3-21.6 m	15.2 - 21.3 m
Batavia	1.25 m	1.5 m	1.5 m	2.35 m
Anyer 4th Point	20-28 m	26-44m	13.3-18 m	10 m

3.2. Tsunami Arrival Time

From eye witness accounts we obtain the arrival time of tsunami generated by the Krakatau eruption. The simulated tsunami arrival time and the reported arrival time at eight locations are shown in Table 2. Comparison of the simulated arrival time and the observed arrival time of tsunami at Betung Bay show that the models are about 60 minutes late. A report from the Besse ship that sailed toward Sunda strait says that they felt an unusual current with a speed of 12 knot at 10.02 AM. This report suggests that the primary eruption at 10.00 AM may not be the only eruption that generated a tsunami around Sunda Strait. From these facts, we speculate that the tsunami that was observed at 10.18 AM in Betung Bay was not generated by the Krakatau primary eruption.

The tsunami arrival time is simulated by using 10.00 AM as the initial time of tsunami propagation. By neglecting the observation at Betung Bay, the delays of simulated tsunami

arrival times from scenario II are between -2 and +15 min (Table 3). The result shows that the simulated arrival time from scenario II are closer to the observation compare to the other scenarios.

Table 2. Tsunami arrival time (local time)

Locations	Observed	Scenario I	Scenario II	Scenario III
Betung Bay	10.18	11.16	11.22	11.19
Kalianda	-	10.48	10.48	10.35
Vlakke Hoek lighthouse	10.30	10.27	10.28	10.25
Merak	10.32	10.51	10.47	10.58
Panaitan Island	-	10.23	10.26	10.28
Caringin	10.30	10.43	10.40	10.47
Batavia	12.30	12.50	12.44	12.52
Anyer 4th Point	-	10.36	10.33	10.38

Table 3. Delay of the simulated arrival timewith respect to observation

Locations	Scenario I (min)	Scenario II (min)	Scenario III (min)
Betung Bay	+58	+64	+61
Kalianda	-	-	-
Vlakke Hoek lighthouse	-3	-2	-5
Merak	+19	+15	+26
Panaitan Island	-	-	-
Caringin	+13	+10	+17
Batavia	+20	+14	+22
Anyer 4th Point	-	-	-

4. CONCLUSIONS

The realistic caldera model of scenario III gives good result on the simulation of tsunami run-up. The cylinder shaped caldera model of scenario II gives good result on the calculation of tsunami arrival time.Tsunami simulation using the collapse of caldera as the generating force is able to explain the arrival time and run-up of the tsunami caused by the 1883 Krakatau eruption. The early tsunami recorded in Betung Bay suggests that tsunami was also generated by smaller eruption on August 27, 1883 before the primary eruption at 10.00 AM.

REFERENCES

Decker,R.W., and Hadikusumo D., (1961), Result of the 1960 Expedition to Krakatoa. Journal of Geophysics, 16, 267-297.

Heliker, (1990), Volcanic and Seismic Hazards on the Island of Hawaii, USGS General Interest Publication.

Hendervari, (1979), The relationship Between Tectonic Earthquakes and Volcanic Eruptions with Particular Reference to Santorini (Aegean Sea) and Indonesia. Geologie en Mijnbouw, 58(2), 213-224.

Johnson J. M., (1999), Heterogenous coupling along Alaska-Aleutians as inffered from tsunami, seismic, and geodetic inversions, Advances in Geophysics, 39, 1-116.

Kawamata, S., F.Imamura and N.Shuto, (1993), Numerical Simulation of The 1883 Krakatau Tsunami, Proceeding of XXV Congress of International Association for Hydraulic Research, Vol.IV, 24-31.
Latief, H., Nanang T. Puspito., Imamura, (2000), Tsunami Catalog and Zoning in Indonesia, Journal of Natural Disaster, 22, 25-43.
Nakamura, S, (1984), A numerical tracking of the 1883 Krakatau tsunami, Science of Tsunami Hazards, 2, 41-54.
Nomanbhoy, N and Satake K., (1995), Generation mechanism of tsunamis from the 1883 Krakatau eruption, Geophys. Res. Letters, 22, 509-512.
Simkin, T and Fiske, R. S. (1983), Krakatau 1883 Eruption and its effects, Smithsonian Institution Press, Washington, D.C.
Verbeek, R.D.M. (1885), Krakatau. *Uitgegeven Op Last Van Zune Excellentie Den Gouverneur-Generaal Van Nederlandsch-Indie*, Batavia Landsdrukkerij.

EARTHQUAKE-RESISTANT CHARACTERISTICS OF INDONESIAN TRADITIONAL TIMBER HOUSES

Ali Awaludin

Instructor, Laboratory of Structures
Department of Civil and Environmental Engineering, Gadjah Mada University
Grafika 2, UGM campus, Yogyakarta 55281, Indonesia
E-mails: ali@tsipil.ugm.ac.id, ali_hokkaido@yahoo.com

Many traditional houses that primarily built from timber have been found to survive even after many earthquakes. One example of these traditional houses is Omo Hada (see Fig. 1), an indigenous house of Nias people at the northern part of Nias Island. Omo Hada house (which was built some 200 years ago) had very light roofing system but massive wood members at the bottom, below the floor and above the ground. Another example is Joglo house which is often found in Yogyakarta and surrounding cities. The impressive Masjid Gedhe of Yogyakarta (see Fig. 2), which was constructed about 250 years ago, adopts the Joglo system. Joglo houses are generally characterized by four wooden columns at the center that are simply placed (sometimes with a notch) on the stone foundation and are connected at the top to multiple timber beams for their lateral stability. The size of the four columns is much larger than the other columns, the columns placed at perimeter. The latest seismic hazard map divides Indonesia into six zones where Nias Island is included in zone 6 with ground acceleration of 0.33*g* and Yogyakarta is located in zone 4 with ground acceleration of 0.24*g*, for dense soil basis. (*g* is gravitational acceleration, 9.8m/s^2)

Omo Hada and Joglo houses (and probably most of traditional houses) used mortise and tenon joint system in their connections, for instance, beam-column joints. This joint system, which is probably the oldest carpentry technique, is also very common to the traditional architecture of many other countries such as Japan, European countries, and etc. In this system no steel fastener is used but mortise member or tenon member has an extent for interlocking purpose. In combination with high quality and large cross-section of wood members (which were not difficult during that time), the mortise-tenon joint system provides timber structures with more lateral integrity to resist the lateral forces of earthquakes. Great frictional resistance or damping among the mortise-tenon joint members absorbs most of the earthquake energy. This behavior is much similar to dynamic performance of log houses in which all log layers response uniformly as a massive body below certain peak ground acceleration (PGA). The concept of frictional damping as passive energy dissipation system has been applied recently in various friction damper devices of steel or concrete (frame) constructions. Though there is little impact to cost, the resulting structures will be less susceptible to structural and non-structural damages due to earthquake.

Another interesting feature of these houses is about their column-foundation boundary. The columns are not strongly connected to the foundation but they are just simply placed (or with a notch) on the stone foundation. In this regard, mass or weight of the upper structure and frictional coefficient (between timber column and stone foundation) are the two important parameters. When frictional or Coulomb damping at contact condition is exceeded, there will be a permanent slip between the column and foundation. The slip may be relatively small considering the massive weight of these traditional houses and it would vanish or amplify when the next earthquake comes. However, it will not increase when the notch works. Here the notch acts as a flexible stopper just like in a base-isolation system. Since the notch is

usually small, the column-foundation interaction can be assumed as a pin support so that large lateral displacement (sway) of the upper structure becomes possible.

Besides those earthquake-resistant aspects, Omo Hada has diagonal members or bracing made from round (solid) wood placed above the ground and below the floor. Bracing members (in two directions) brace the columns and allow the natural flexible of wood structures to deform just enough to absorb the earthquake energy without being disconnected. In addition, the four main columns of Omo Hada that support the roof system are laterally reinforced by diaphragm action of the wooden floor. These two traditional houses have different earthquake-resistant levels and by tradition they are located at two areas with different seismic hazard intensities.

Figure 1
Omo Hada of Nias Island (photos, courtesy of Feri Latief, 2007)

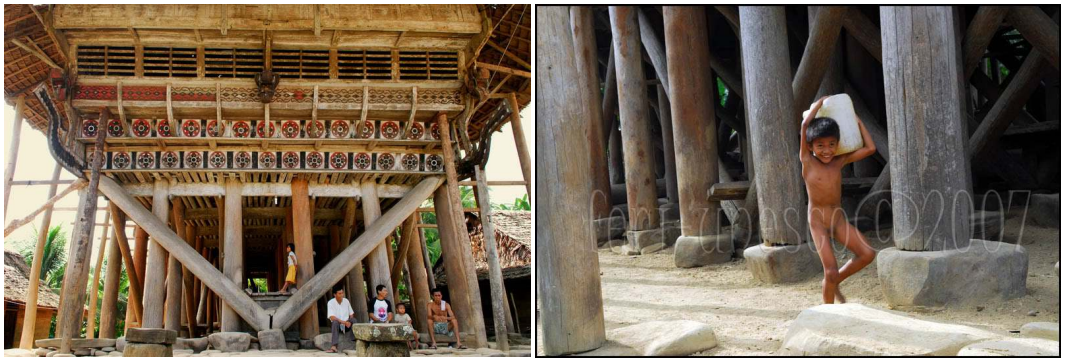

Figure 2
Joglo System of Masjid Gedhe, Yogyakarta (photos, courtesy of Virgina Veryastuti, 2008)

THE EFFECT OF CONTACT ANGLE POLYDISPERSITY ON CAPILLARY BEHAVIOR IN POROUS MEDIA

Esti Puspitaningrum[1,*] and Shusaku Harada[2]

[1,2] Graduate School of Engineering, Division of Sustainable Resources Engineering, Hokkaido University, Japan.
**E-mail:* fistek_29600@yahoo.com

ABSTRACT: A study of wicking behavior between cylinders with different contact angles is fundamental and may provide a better understanding of capillary penetration of liquid into more complicated structures such as mixed-soil. A model formed by two closely spaced parallel cylinders whose contact angle may be identical or different was employed in this paper. The capillary rise between those cylinders, which was estimated by force balance analysis, has good agreement with the experiment results. The analysis is extended to a more complicated system. Capillary pressure vs. saturation curves were obtained for bundles of parallel pores with contact angle distribution. We use two models of pore, circular and curved triangular. The result for curved triangular model is qualitatively similar to the one observed for real porous media, while the result for the circular pore model seems to be idealistic.

Keywords*: capillary pressure, saturation degree, polydispersity in contact angle, porous media.*

1. INTRODUCTION

The flow behavior of two or more immiscible fluids in porous media is of paramount importance in petroleum migration and recovery, soil hydrology, wicking, detergency, etc. One of the important parameters affecting the multifluid flow behavior is wettability. Wettability is generally represented by contact angle θ, i.e., the angle at which wetting phase and non wetting phase interface meet the solid surface. Contact angle is specific for any given system and is determined by the interactions across the three interfaces (interfaces of solid, wetting phase and non wetting phase). Different contact angle gives different effect on multifluid behavior in porous media.

Up to now porous media is always represented by model whose contact angles are identical for all of its pores. This model is over simplified as even a single glass plate has different contact angle at different part. The porous media which may consist of many kinds of material must have at least a range of contact angle values. There are only few experimental investigations are available in this field [1-3]. Most of them only considered capillary behavior in systems whose contact angles were identical. Discussion about capillary between materials whose contact angles are not identical has not been given to most of author's knowledge.

Therefore capillary behavior between materials whose contact angles may be identical or different is examined theoretically and experimentally in this paper. We use cylinders, whose contact angles vary, as the model and examine the wicking behavior between them. And for a better understanding of multifluid flow behavior in porous media, the effect of porous media's polydispersity in contact angle on multifluid flow behavior needs to be investigated. In this paper, we focus on estimating the percentage amount (saturation degree) of wetting phase fluid in porous media whose pores vary in contact angle and the pressure which is needed to remove or place it.

2. CAPILLARY BEHAVIOR BETWEEN CYLINDERS WHOSE CONTACT ANGLES MAY BE IDENTICAL OR DIFFERENT

2.1 Theory

When a sufficient amount of liquid is brought into the gap between two narrowly spaced wettable cylinders, surface tension γ can draw liquid up the gap in a phenomenon known as capillary action (Figure 1a). The height of liquid H above the initial level, which can represent the capillary pressure across the interface, depends on various properties such as cylinders radius, gap distance, and contact angle.

The height of liquid H can be estimated by considering force balance equation as follows. The weight of the liquid wicked in the gap must be supported by the upward force due to surface tension in the meniscus region (Figure 1b). The force due to surface tension consist of two terms: an upward force resulting from the contact of the liquid and the cylinders along AB and CD, and a downward force due to the free vertical liquid surfaces along BC and DA which tend to pull down the liquid column. These forces are expressed by the product of surface tension γ with their arch length. The force balance equation is given as follows.

$$\gamma[\cos\theta_1 AB + \cos\theta_2 CD - (DA + BC)] = \rho_L g A_L H \quad (1)$$

where ρ_L is mass density of liquid, g is gravitational acceleration, θ_1, θ_2 are contact angles and A_L is cross sectional area of liquid column (shadowed area in Figure 1b). AB ($= 2R_W a_1$), CD ($= 2R_W a_2$) and DA=BC ($= r[\pi - a_1 - \theta_1 - a_2 - \theta_2]$) are arc length of each interface (The meaning of each symbols is described in Figure1b). In Eq.(1) we neglect the small volume of saddle shape liquid just below the liquid front, therefore the system must satisfy $H \gg R_W$.

We can also express the capillary rise by using the cylinder radius R_W and the radius of menisci r as follows [2].

$$H = \frac{R_W}{r}\frac{\gamma}{\rho_L g R_W} \quad (2)$$

The cross sectional area A_L is obtained from geometric consideration and is given by:

$$A_L/(R_W)^2 = 2r/R_W [\sin(a_1) \cos(a_1+\theta_1) + \sin(a_2) \cos(a_2+\theta_2)] - [a_1 + a_2 - \cos(a_1)]$$

Moreover, the following two equations with respect to the radius of menisci r are also derived by geometric analysis.

$$\frac{r}{R_W} = \frac{2 + 2\frac{d}{R_W} - [\cos a_1 + \cos a_2]}{[\cos(a_1+\theta_1) + \cos(a_2+\theta_2)]} \quad (4)$$

$$\frac{r}{R_W} = \frac{\sin a_1 - \sin a_2}{[\sin(a_2 + \theta_2) - \sin(a_1 + \theta_1)]} \quad (5)$$

We can obtain the value of r/R_W and then the value of H from Eq.(1) to Eq.(5) for given values of γ, ρ_L, g, θ_1, θ_2, and d/R_W.

2.2 Verification of Theory by Experiment

A series of experiments was conducted to verify the theory. The samples, glass cylinders with radius R_W=1.25 mm, was cleaned by using 70% ethanol solution and then dried. Then two selected cylinders were held vertically in water by using metal holder. The resulting capillary rise was observed by digital microscope camera and measured directly by image processing (Figure 2a). The normalized curvature of meniscus R_W/r (inverse of normalized meniscus radius) was calculated based on Eq.(2) with measured surface tension γ =0.07013 N/m. All experiments were conducted at temperature 20 ± 2°C. Contact angles at outside surface of each cylinder were measured directly at the points where wetting phase menisci exist, after directly capture side view of system by microscope. Figure 2b shows result of image processing to measure contact angle.

Table 1 shows the measured contact angles (θ_1 and θ_2) with respect to 17 pairs of cylinders and the values R_W/r obtained from experiment and theory. As can be seen in Table 1, the contact angle of glass cylinder varies widely and the capillary rise H is greatly influenced by the variance of contact angles. Figure 3 indicates the comparison between experimental and theoretical results. The experiment results show that the theory has good agreement with the test results, not only for cylinders with the same contact angle (Figure 3a), but also for cylinders with different values of contact angle as shown in Table 1 and Figure 3(b).

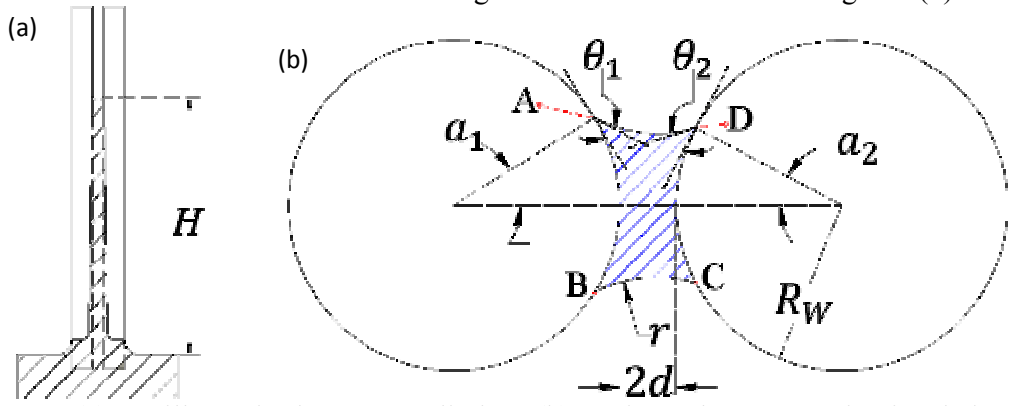

Figure 1 (a) Capillary Rise between Cylinders, (b) Horizontal Cross-Section just below the Liquid Meniscus

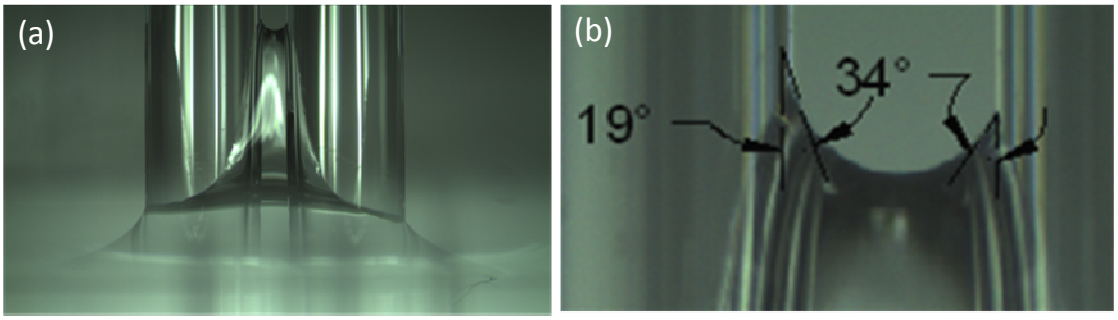

Figure 2 Photos of Capillary Rise between Cylinders in Experiments. (a) Front View, (b) The Meniscus of the Liquid Front

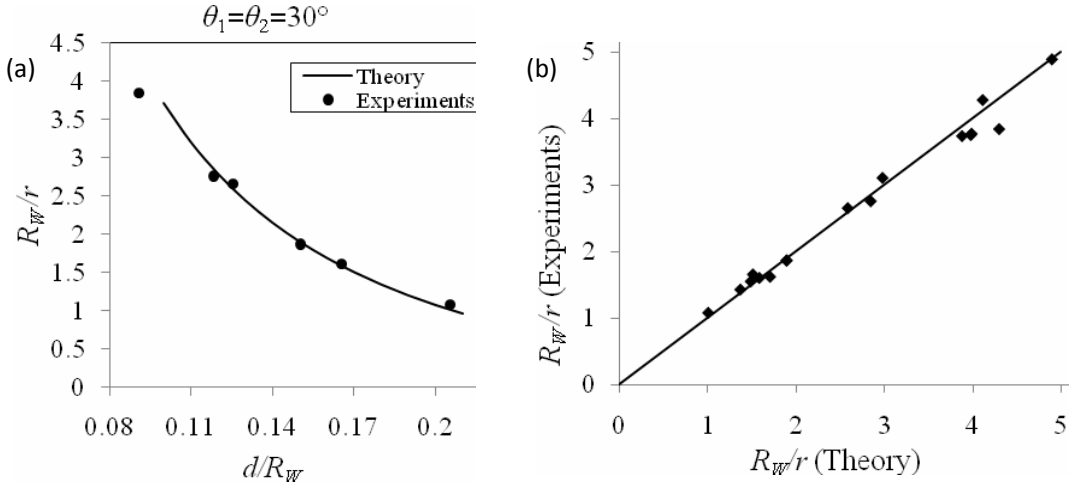

Figure 3 Comparisons between Experiments and Theory. (a) Cylinders Distance vs. Normalized Curvature for Cylinders with $\theta = 30°$, (b) Linear Fit of Theory vs. Experiment Results for Normalized Curvature with Various Contact Angles

Table 1 Experimental Results of Capillary Rise between Cylinders

No	θ_1	θ_2	$\frac{d}{R_W}$	H (mm)	R_W/r Theory	R_W/r experiment	No	θ_1	θ_2	$\frac{d}{R_W}$	H (mm)	R_W/r Theory	R_W/r experiment
1	30	30	0.2054	6.2	1.013	1.084	10	45	52	0.0765	17.8	2.983	3.113
2	31	54	0.1334	8.2	1.376	1.434	11	31	32	0.0949	21.4	3.881	3.742
3	29	53	0.1330	8.9	1.493	1.556	12	29	29	0.0970	21.5	3.980	3.760
4	30	46	0.1432	9.5	1.518	1.661	13	29	31	0.0954	21.6	3.990	3.777
5	30	30	0.1653	9.2	1.591	1.609	14	34	47	0.0766	24.5	4.115	4.284
6	30	34	0.1534	9.3	1.712	1.626	15	31	39	0.0763	28.0	4.898	4.896
7	30	30	0.1503	10.7	1.899	1.871	16	30	30	0.0907	22.0	4.301	3.847
8	30	30	0.1256	15.2	2.591	2.658	17	30	30	0.1503	10.7	1.900	1.871
9	30	30	0.1185	15.8	2.849	2.763							

3. POROUS MEDIA WITH POLYDISPERSITY IN CONTACT ANGLE

In the previous section, we demonstrated how the contact angle affects the capillary behavior of liquid and ascertained the validity of force balance model in a simple case, i.e., capillary rise between two cylinders. Here we discuss the role of contact angle on drainage and imbibition processes in porous media.

3.1 Princen's Single Pore Model

In general, the pressure required for draining liquid from porous media (or penetrating into porous media) is determined by the capillary pressure P which causes by the surface tension. The liquid flow through porous media, regardless of how complex the porous structure is, can always be simplified by a single capillary tube flow model [3–9]. Princen [2] studied the imbibition and drainage behaviors of wetting phase (e.g. water) through non wetting phase (e.g. air) by two types of single pore model, i.e., a circular pore and a curved triangular pore. Figure 4 indicates the pressure for drainage and imbibition vs. saturation degree of (P –S_W curve) in a circular pore (a) and in a curved triangular pore (b). He derived these results by a similar force balance model as described in previous section. It is found from Figure 4 that there is no drainage – imbibition hysteresis in circular pore. On the other hand, the hysteresis occurs in curved triangular pore. In drainage process, when the pressure of non wetting phase exceeds the drainage pressure P_d, the wetting phase goes out from the pore. On the contrary, the wetting phase penetrates into the pore with decreasing the pressure of non wetting phase. When the pressure reaches the imbibition pressure P_i, the pore is saturated by wetting phase.

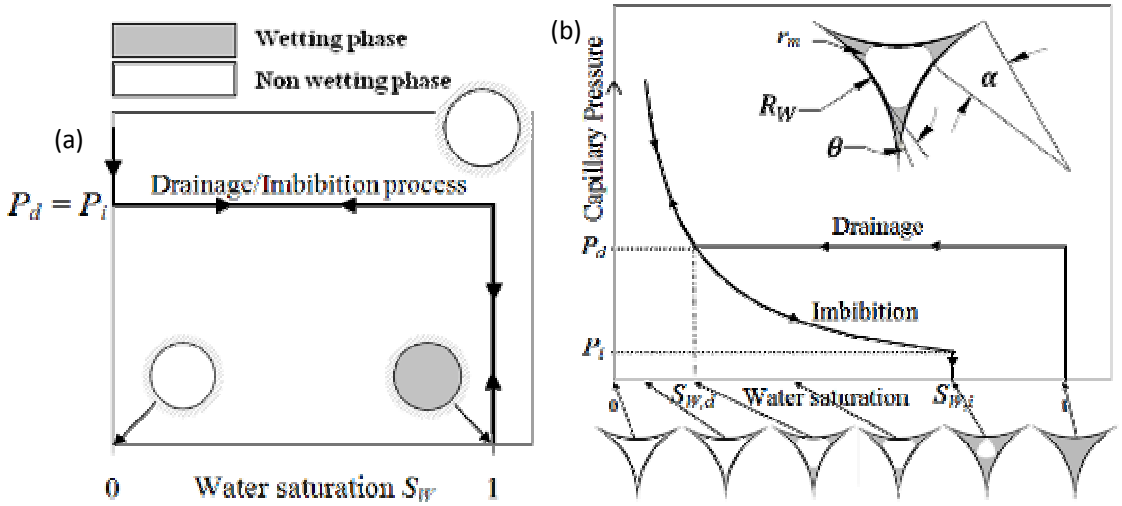

Figure 4 Pressure vs. Saturation Degree (P –S_W Curve) for Drainage and Imbibition Processes (a) in a Circular Pore Model (b) in a Curved Triangular Pore Model [2]

Princen has derived the value of $S_{W,d}$, which is wetting phase saturation degree at which the pressure equal to P_d for some values of contact angle θ [2]. The corresponding wetting phase saturation S_W is shadowed area divided by total area inside pore and is given by:

$$S_W(\theta) = \frac{6}{\left(\sqrt{3}-\frac{\pi}{2}\right)}\left\{\frac{r_m}{R_W}\sin\alpha\cdot\sin\left(\frac{\pi}{2}-\alpha-\theta\right)-\frac{{r_m}^2}{2{R_W}^2}\left(\frac{\pi}{2}-\alpha-\theta-\sin\left(\frac{\pi}{2}-\alpha-\theta\right)\cos\left(\frac{\pi}{2}-\alpha-\theta\right)\right)\right. \quad (6)$$

where menisci radius r_m is related to angle α according to following equation:

$$r_m/R_w = (1-\cos\alpha)/\cos(\theta+\alpha) \tag{7}$$

The capillary pressure for system illustrated in Figure 4 is $P = \gamma/r_m$.

3.2.Model of Contact Angle Polydispersity in Bundle of Parallel Pores

In this section, the final purpose is to obtain curve of normalized pressure vs. wetting phase saturation degree in bundle of pores with distribution of contact angle. We set all pores have the same volume and vary the contact angle from $\theta_1 = (a - 0.5b)$ to $\theta_2 = (a + 0.5b)$ between 0° and 90°. Where *a* is a median of contact angle and *b* is a distribution width. The value of *b* is between 0° and 90°. Higher value of *b* means higher level of polydispersity.
Then for the sake of illustration, the number of pores with contact angle θ in a bundle of parallel pores is defined by Gaussian distribution:

$$N(\theta) = 1000\frac{1}{\sqrt{2\pi}}e^{-\frac{[z(\theta)]^2}{2}} \tag{8}$$

where

$$z(\theta) = \left(7\frac{\theta - a}{b} - 3.5\right) \tag{9}$$

The total number of pores whose contact angle is or between θ_1 and θ is defined by:

$$D(z(\theta)) = \int_{z(\theta_1)}^{z(\theta)} N(\theta)dz \tag{10}$$

Thus the total number of pores N_T is calculated as follows.

$$N_T = \int_{-\infty}^{\infty} N(\theta)dz = D(z(\theta_2)) = \int_{7\frac{\theta_1 - a}{b} - 3.5}^{7\frac{\theta_2 - a}{b} - 3.5} 1000\frac{1}{\sqrt{2\pi}}e^{-\frac{z^2}{2}}dz \tag{11}$$

3.3 *P*-S_w Relationship of a Bundle of Circular Pores

For circular pore, there is no hysteresis between drainage and imbibition processes. Their $P - S_W$ curves are overlapping, as seen in Figure 5a. Therefore both processes can be examined in one analysis. In circular pore model, the imbibition pressure P_i and drainage pressure P_d is equal to $2\gamma\cos\theta/R$ in which R is pore radius. Then the normalized pressure for circular pore with contact angle θ is:

$$\tilde{P}_i(\theta) = \tilde{P}_d(\theta) = \frac{2\gamma\cos\theta/R}{2\gamma/R} = \cos\theta \tag{12}$$

where $\tilde{P}$ is the normalized pressure by $2\gamma/R$,
When we apply $\tilde{P}$ which is equal to $\tilde{P}_d(\theta)$ to pores, the pores with contact angle less than θ will still fully filled by wetting phase and pores with contact angle larger than θ will empty of wetting phase. Therefore the total saturation degree $S_{W\text{total}}$ will be:

$$S_{W\text{total}} = \frac{D(z(\theta))}{D(z(\theta_2))} \tag{13}$$

By choosing θ as independent variable, defining the median of contact angle *a* and the distribution width *b*, and using Eq.(8) to Eq.(13), we will obtain the value of normalized drainage pressure and saturation degree $S_{W\text{total}}$ for bundle of circular pores with a certain distribution of contact angle.

3.4 *P*-S_w Relationship of a Bundle of Curved Triangular Pores

For curved triangular pores model, the drainage pressure of pore whose contact angle is equal to θ , $P_d(\theta)$, can be obtained as $\gamma/r_d(\theta)$ where $r_d(\theta)$ is the menisci radius at the pressure P_d (see Figure 4b) [2]. The drainage pressure normalized by γ/R_w is given as follows.

$$\tilde{P}_d(\theta) = \frac{\gamma/r_d(\theta)}{\gamma/R_w} = \frac{R_w}{r_d(\theta)} \tag{14}$$

When we apply $\tilde{P}_d(\theta)$ to pores, all pores with contact angle less than θ will still fully filled by wetting phase and the rest pores will drain. Therefore, when we apply normalized pressure $\tilde{P}_d = R_w/r_d(\theta)$, the total saturation degree of wetting phase $S_{W\text{total}}$ can be calculated as follows.

$$S_{W\text{total}} = \frac{D(z(\theta))}{N_T} + \frac{\sum_{\theta_i=\theta}^{\theta_2} S_W(\theta_i) \times \left(D(z(\theta_{i+1})) - D(z(\theta_i))\right)}{N_T} \tag{15}$$

where $\theta_{i+1} = \theta_i + \Delta\theta$. $S_W(\theta_i)$ is defined according to Eq.(6) and Eq.(7) with $r_m = r_d(\theta)$. $D(z(\theta_{i+1})) - D(z(\theta_i))$ means the total number of pores whose contact angle is between θ_i and θ_{i+1}. As in circular model, by having θ as independent parameter, we will obtain the value of normalized pressure and saturation degree $S_{W\text{total}}$ for a bundle of triangular pores in drainage process.

Next we consider the imbibition process. We can calculate normalized imbibition pressure of pore with contact angle θ for imbibition process from Eq.(7) as follows.

$$\tilde{P}_i(\theta) = \frac{R_w}{r_i(\theta)} \tag{16}$$

where $R_w/r_i(\theta)$ is normalized curvature of menisci at imbibition for pore with contact angle θ , which can be defined as:

$$\frac{R_w}{r_i(\theta)} = \frac{\cos(\theta + \alpha_{\max})}{(1 - \cos\alpha_{\max})} \tag{17}$$

where $\alpha_{\max}$ corresponds to the maximum α in which the imbibition process end (see Figure 4b). Based on imbibition schematic, when we apply normalized pressure equal to $\tilde{P}_i(\theta)$ to pores, pores with contact angle less than θ will have wetting phase saturation equal

to their imbibition saturation $S_{W,i}(\theta_i)$ and the rest pore will have wetting phase saturation equal to $S_W(\theta_i)$ which can be obtained according to Eq.(6) and Eq.(7) with $r_m = r_i(\theta)$. Therefore the total saturation becomes:

$$S_{W\text{total}} = \frac{\sum_{\theta_i=\theta_1}^{\theta} S_{W,i}(\theta_i) \times \left(D(z(\theta_{i+1})) - D(z(\theta_i))\right)}{N_T} + \frac{\sum_{\theta_i=\theta}^{\theta_2} S_W(\theta_i) \times \left(D(z(\theta_{i+1})) - D(z(\theta_i))\right)}{N_T} \quad (18)$$

where

$$S_{W,i}(\theta_i) = \frac{6}{\left(\sqrt{3} - \frac{\pi}{2}\right)}\left\{\frac{r_i(\theta_i)}{R_w} \cdot \frac{1}{2} \cdot \sin\left(\frac{\pi}{3} - \theta_i\right) - \frac{1}{2}\left(\frac{r_i(\theta_i)}{R_w}\right)^2 \left(\frac{\pi}{3} - \theta_i - \sin\left(\frac{\pi}{3} - \theta_i\right) \cdot \cos\left(\frac{\pi}{3} - \theta_i\right)\right) - \frac{1}{2}\left(\frac{\pi}{6} - \frac{1}{4}\sqrt{3}\right)\right\} \quad (19)$$

$r_i(\theta_i)/R_w$ can be calculated based on Eq.(17) with θ is replaced by θ_i. If the applied normalized pressure is higher than $\tilde{P}_i(\theta_1)$, no pore is in entrapment condition, $S_{W,i}(\theta_i) = 0$. As in drainage process, by having θ as independent parameter, we will obtain the value of normalized pressure and saturation degree $S_{W\text{total}}$ for a bundle of triangular pores in imbibition process.

3.5 Results and Discussion

In order to investigate the effect of contact angle polydispersity, we estimated multifluid flow behavior by using two types of pore models described in the previous section. We set three kinds of distribution of contact angle in a bundle of pores as indicated Figure 7(a).

Figure 7(b) shows the results of $P - S_W$ curve for circular pore model. In a bundle of circular pores, the polydispersity of contact angle only gives one effect, i.e., as the polydispersity increases, the sharp features of $P - S_W$ curve are smoothed out. Although these smoothed features are closer to the one observed for real porous media, there is still no hysteresis.

Figure 7(c) shows the results of $P - S_W$ curve for curved triangular model. In a bundle of triangular pores, there are some other trends clearly revealed: (1) As the polydispersity in contact angle increases, the hysteresis becomes more pronounced; (2) The polydispersity in contact angle gives small but clear effect on saturation degree $S_{W,i}$ and $S_{W,d}$. These features are qualitatively similar to the observation for real porous media. It is also found from Figure 7(c) that there is no effect of contact angle polydispersity at capillary pressure equal to $P_d(45°)$. This is as expected, since the distributions are centered at $\theta = 45°$.

4. CONCLUSION

We theoretically studied the capillary behavior in gap or pores by force balance models. Firstly we demonstrated how the contact angle affects the capillary behavior of liquid in a simple case, i.e., capillary rise between two cylinders. Next we extended the model to more complicated system and discussed the role of contact angle on drainage and imbibition processes in porous media. We showed that the polydispersity in contact angle have contribution in the change in capillary behavior of porous media. As suggested by previous

studies [2-3], the pore model with angular cross-section show many of the qualitative features exhibited by real porous media.

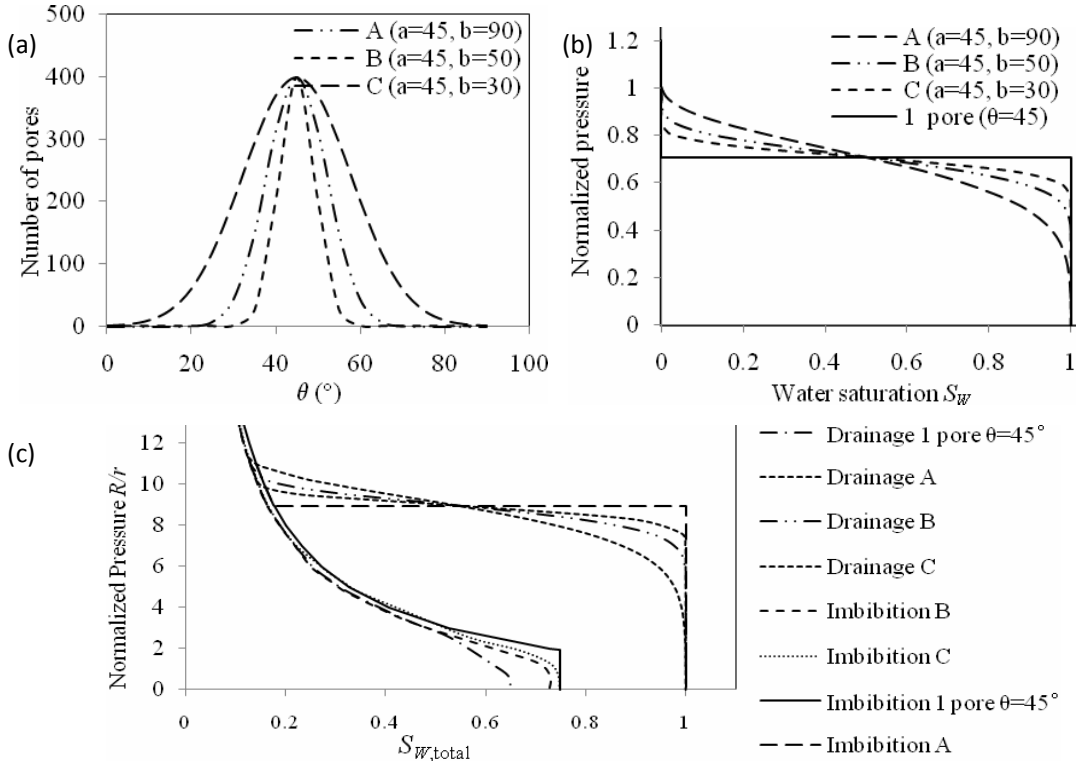

Figure 7 (a) Illustration of Contact Angle Polydispersity. Pressure vs. Saturation Degree of Bundle of Pores with Contact Angle Polydispersity for (b) Circular Pore Model and (c) Curved Triangular Pore Model

REFERENCES

[1] Liu, T., Choi, K.F. and Li, Y., (2007), Capillary rise between cylinders, *J. Phys. D: Appl. Phys.*, Vol. 40, 5006.

[2] Prince, H.M. (1992), Capillary pressure behavior in pores with curved triangular cross-section: Effect of wettability and pore size distribution, *J. Colloid Int. Sci.,* Vol. 65, 221.

[3] Mason, G. and Morrow, N.R. (1991), Capillary behavior of a perfectly wetting liquid in irregular triangular tubes, *J. Colloid Int. Sci.,* Vol. 141, 262.

[4] Scheidegger, A.E. (1974), The physics of flow through porous media. Toronto: University of Toronto Press.

[5] Amico, S.C. and Lekakou, C. (2002), Axial impregnation of a fiber bundle: 1. Capillary experiments, *Polym. Compos.*, Vol. 23, 249.

[6] Amico, S.C. and Lekakou, C. (2002), Axial impregnation of a fiber bundle: 2. Theoretical analysis, *Polym. Compos.*, Vol. 23, 264.

[7] Hollies, N.R.S., Kaessinger, M.M. and Bogaty, H. (1956), Water transport mechanisms in textile materials: I. The role of yarn roughness in capillary-type penetration, *Text. Res. J.*, Vol. 26, 829.

[8] Hollies, N.R.S., Kaessinger, M.M., Watson B.S. and Bogaty, H. (1957), Water transport mechanisms in textile materials: II. Capillary-type penetration in yarns and fabrics, *Text. Res. J.*, Vol. 27, 8.
[9] Marmur, A. and Cohen, R.D. (1997), Characterization of porous media by the kinetics of liquid penetration: the vertical capillaries model, *J. Colloid Int. Sci.*, Vol. 189, 299.
spective future as medicinal therapy for diabetes.

INDONESIAN TRADITIONAL HERBS FOR DIABETES

Maria D.P.T.Gunawan-Puteri[1], Tomohiro Ieyama[1], Stella Kristanti[2] and Jun Kawabata[1]

[1]Laboratory of Food Biochemistry, Division of Applied Bioscience, Graduate School of Agriculture, Hokkaido University, Japan
[2]Food Science and Technology, Faculty of Agriculture Technology, Bogor Agricultural University, Indonesia
Corresponding e-mail: newflorentinamd@yahoo.com

ABSTRACT: Diabetes mellitus is affecting nearly 10% of the population every year. In 1997, an estimated 124 million people worldwide have diabetes, 97% of them are suffering from non insulin dependent diabetes mellitus or diabetes type 2 (DM2). Indonesia is the 4th country after India, China, and United States which have the largest number of diabetic patients. One of the studies related to this field is study on anti-diabetes from natural source. Natural products are potential resources for future medicine if they meet scientific and regulatory tests. As an archipelago country with low income per capita, most of Indonesian people have limited access to modern treatment and often consume local or indigenous medicines called jamu. In this paper, we briefly discuss application of jamu as source of α-glucosidase inhibitors in relation with their prospective future as medicinal therapy for diabetes.

Keywords: *Diabetes, Indonesia, Jamu, Medicinal herbs*

1. α-GLUCOSIDASE INHIBITORS AS DIABETES TREATMENT

Diabetes mellitus (DM) is a metabolic disorder characterized by a congenital (DM1) or acquired (DM2) inability to transport glucose from the bloodstream into cells. DM2 and associated cardiovascular diseases and cancer are an increasing problem around the globe, especially in the developed world (Beaglehole & Yach, 2003). A worldwide survey reported that diabetes mellitus is affecting nearly 10% of the population every year (Vetrichelvan, Jagadeesan, & Uma Devi, 2002). Diet and exercise are the first steps in the treatment of DM2. But if these measures alone fail to sufficiently control blood glucose levels, starting oral drug therapy is recommended.

Carbohydrates are the major constituents of the human diet. α-Glucosidase (EC 3.2.1.20), located in the brush-border surface membrane of intestinal cells, has drawn a special interest of the pharmaceutical research community because it was shown that the inhibition of its catalytic activity led to the retardation of glucose absorption and the decrease in postprandial blood glucose level (Robinson, Begovic, Rhinehart, Heineke, Ducep, Kastner, *et al.,* 1991; Braun, Braver, & Withers, 1995; Dwek, Butters, Platt, & Zitzmann, 2002). α-Glucosidase inhibitors (AGIs) reversibly inhibit α-glucosidases such as maltase and sucrase in intestine, consequently delaying the absorption of sugar from the gut (Campbell, White, & Campbell, 1996). This indicates that effective AGIs may serve as chemotherapeutic agents for clinic use in the treatment of diabetes and obesity.

AGIs might be a reasonable option as first-line drug in the treatment of patients with DM2 as it specifically targets postprandial hyperglycemia, a possible independent risk factor for cardiovascular complications (Ceriello, 2005). Intensive glucose control in DM1 patients led to an approximate 60% reduction in the risk of disease progression in eyes, kidneys, and nerves (Diabetes Control and Complication Trial Research Group, 1993) while 10 years of improved glucose control in DM2 resulted in a 25% reduction in microvascular complications

(UKPDS, 1998). Although rare cases of hepatic injury were described, AGIs are expected to cause no hypoglycemic events or other life-threatening events, even at overdoses, and cause no weight gain (Chiasson, Josse, Gomis, Hanefeld, Karasik, & Laakso, 2003).

Carbohydrate-mediated biomolecular interactions play key roles in various pathological processes. For example, toxins, bacteria and viruses enter target cells by initial adhesion to host cells through interactions of the pathogenic proteins with host cell-surface glycans. Tumor metastasis takes place through binding of O-linked glycans, often overexpressed on cancer cell surfaces, to selectins of host platelets, leukocytes or endothelial cells. Leukocyte recruitment to sites of inflammation is mediated by initial selectin–sialyl Lex interactions between the circulating leukocytes and the endothelial cells. These catalytic roles in digesting carbohydrate substrates also makes α-glucosidase a therapeutic target for the other carbohydrate-mediated diseases including cancer (Humphries, Matsumoto, & White, 1986), viral infections (Mehta, Zitzmann, Rudd, Block, & Dwek, 1998; Karpas, Fleet, Dwek, Petursson, Namgoong, & Ramsden, 1988), and hepatitis (Zitzmann, Mehta, Carrouee, Butters, Platt, McCauley, *et al*., 1999).

2. INDONESIAN TRADITIONAL HERBS AS POTENTIAL SOURCE OF α-GLUCOSIDASE INHIBITORS

Indonesian traditional herbs or jamu is an integrated part of Indonesian people. Eventhough there are some misleading conception that jamu are strange plants that are mixed in strange way to give unknown effect, actually jamu consist of many plants that we consumed regularly also. As examples, cabbage that is used traditionally for alcohol intoxication antidote and cauliflower that is used for depressant are common menu in many Indonesian people diet. Interesting fact about Jamu and Indonesian people is that the same ingredients are found on their dining table, as well as on their face and their body. For Indonesian people, food, cosmetic, and medicine are overlapping one to each other.

Due to overall improvement in the promotion of health benefits derived from functional food, consumer acceptance of natural sourced treatment and prevention is increasing day by day. Natural products are potential resources for future medicine if they meet scientific and regulatory tests (Koop, 2002). In order to reveal novel natural sourced treatments, it is more efficient to screen plants used in traditional medicine, as these yield a much higher output of interesting substances than plants sampled at random (Koop, 2002). It is because most of the plant materials that have been used for generations for treatment are reasonably safe (de Padua, Bunyapraphatsara, & Lemmens, 2002).

Many efforts have been made searching for effective and safe AGIs from natural materials in order to develop a physiological functional food or lead compounds for antidiabetic (Nishioka, Kawabata, Aoyama, 1998; Yoshikawa, Morikawa, Matsuda, Tanabe, Muraoka, 2002; Matsui, Ueda, Oki, Sugita, Terahara, Matsumoto, 2001). A review has discussed 343 medicinal plant species which have reputation in indigenous medicine or have been scientifically demonstrated (Atta-Ur-Rahman & Zaman, 1989).

As an archipelago country with low income per capita, most of Indonesian people have limited access to modern treatment and often consume local or indigenous medicines. Diabetes mellitus (DM) is one of the diseases that have been treated with plant extracts since

ancient time. Most common jamu ingredients for diabetes treatment are brotowali (*Tinospora crispa*), sambiloto (*Andrographis paniculata*), and pulai (*Alstonia scholaris*)

In Indonesia, there are more than 20,000 species of medicinal plants, but only about 1,000 of them have been recorded and only about 300 species that have been widely utilized in traditional medications (Hariana, 2006). Many of Indonesian medicinal plants potencies are still unrevealed yet. The findings strongly led us to study antidiabetic compounds from Indonesia natural resources as an alternative medicinal food.

3. **α-GLUCOSIDASE INHIBITORS FROM INDONESIAN TRADITIONAL HERBS**

As a continuing part of our screening for AGIs, prospective Indonesian herbs were investigated to determine the antihyperglycemic effect (Gunawan-Puteri, Bhandari, & Kawabata, 2009; Gunawan-Puteri & Kawabata, 2010). Determination of prospective herbs done by *in-vitro* assays to evaluate their inhibitory activities against maltose hydrolysis by rat intestinal α-glucosidases resulted in the finding that crude methanolic extract of *M. tanarius* leaves, *E. americana* bulbs, *Ba. frutescens* stalks, and *Bl. Balsamifera* leaves showed potent inhibitory activities against maltase. Active principles of these herbs were isolated, identified, and submitted for their maltase inhibitory activities. The results were presented as half maximal inhibitory concentration value (IC_{50} value). The IC_{50} value was defined as the concentration of the extract required to inhibit 50% of a-glucosidase activity under the assay conditions.

A 50% aqueous methanol-soluble extracts of each plant were chromatographed using open column chromatography and subsequently purified with preparative HPLC to isolate active principles against α-glucosidase.

Five ellagitannins, mallotinic acid, corilagin, chebulagic acid, and two novel compounds named macatannins A and B were successfully isolated and identified from *M. tanarius* (Figure 1). Chebulagic acid, macatannins A and B have considerably high inhibitory activity against maltase (IC_{50} =1.00 mM, 0.55 mM; and 0.80 mM, respectively) while the other two ellagitannin showed low or no inhibition (less than 50% inhibition in 1.00 mM). Among the isolates macatannins A and B are first time found in *M. tanarius* (Gunawan-Puteri & Kawabata, 2010) while other compounds have been isolated from this plants as well as other plants (Gao, Huang, Xu & Kawabata, 2007; Tabata, Katsube, Tsuma, Ohta, Imawaka, & Utsumi, 2008; Fogliani, Raharivelomanana, Bianchini, Bouraima-Madjebi, Hnawia, 2005)

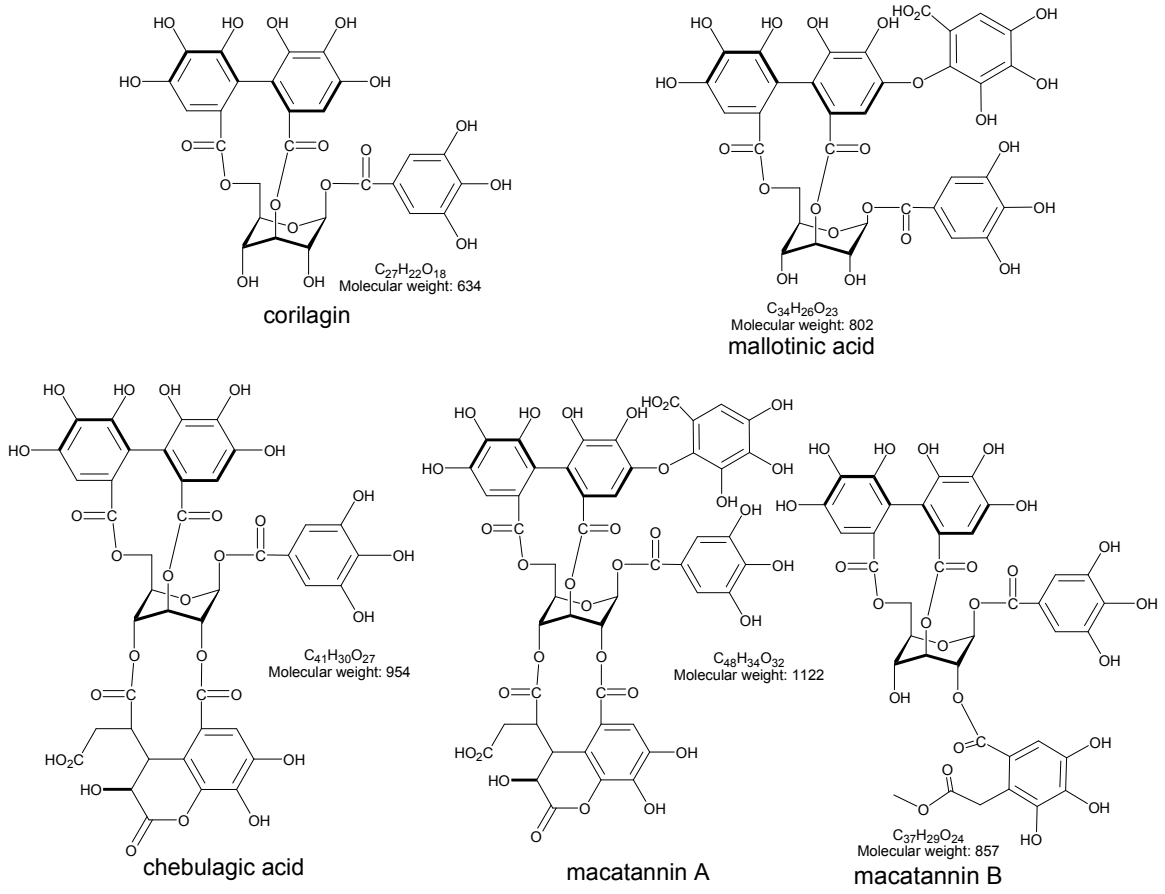

Figure 1. Ellagitanins isolated from *M. tanarius* leaves

Three naphtalenes, eleutherol, eleutherinoside A, and eleuthoside B were isolated from *E. americana* (Figure 2). Eleutherinoside A have high inhibitory activity against maltase (IC_{50} = 0.50 mM while the other compounds showed low or no inhibitory activity. All three naphtalenes have been previously isolated from *E. americana* and other species from the same genus (Shibuya, Fukushima, Ohashi, Nakamura, Riswan, & Kitagawa, 1997; Ketzinel, Rudi, Schleyer, Benayahu, & Kashman, 1996; Paramapojn, Ganzera, Gritsanapan, & Stuppner, 2008)

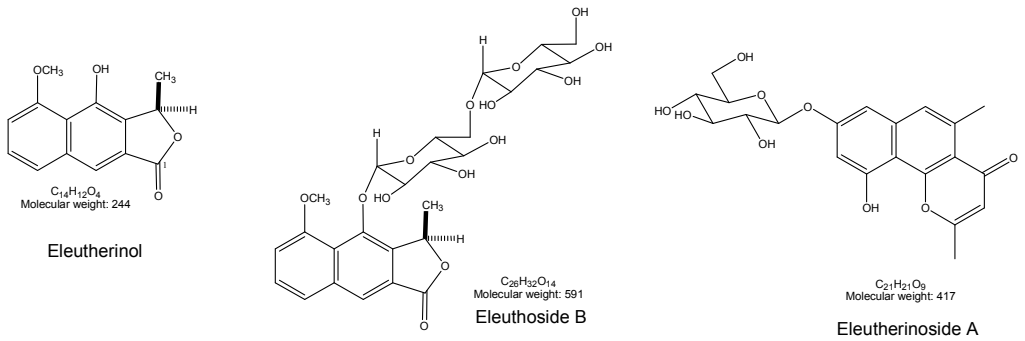

Figure 2. Naphtalenes isolated from *E. americana* bulbs

Purification of active compounds result in the isolation of myricetin-3-*O*-$_L$-rhamnoside and 8-□-*C*-(2-*O*-galloylglucopyranosyl)-5,7-dihydroxy-2-isopropylchromone from *Ba. frutescens* (Figure 3) and also quercetin-3-*O*-galactoside and quercetin-3-*O*-glucoside from *Bl. Balsamifera* (Figure 4). These compounds showed low or no inhibition against maltase.

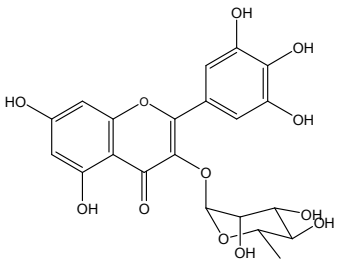

Myricetin-3-*O*-$_L$-rhamnoside

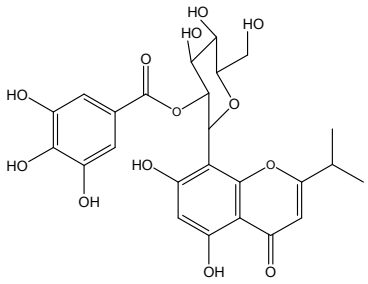

8-beta-C-(2-*O*-galloylglucopyranosyl)-5,7-dihydroxy-2-isopropylchromone

Figure 3. Compounds isolated from *Ba. frutescens* stalks

Compound 8-□-*C*-(2-*O*-galloylglucopyranosyl)-5,7-dihydroxy-2-isopropylchromone was previously isolated also from *Ba. frutescens* (Chung, Kim, Takaya, Terashima, & Niwa, 2004) while myricetin-3-*O*-$_L$-rhamnoside was previously isolated from *Sageretia theezans* (Satake, Kamiya, Saiki, Hama, Fujimoto, Endang, & Umar, 1999). Quercetin-3-*O*-galactoside and quercetin-3-*O*-glucoside also have been previously isolated before (Sakar, Sohretoglu, Ozalp, Ekizoglu, Piacente, & Pizza, 2005; Moco, Tseng, Spraul, Chen, & Vervoot, 2006).

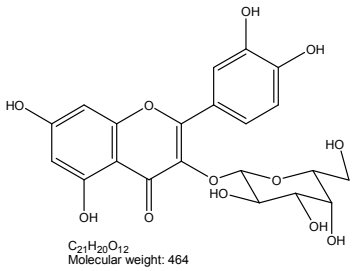

quercetin-3-*O*-galactoside

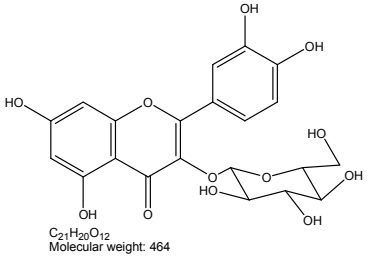

quercetin-3-*O*-glucoside

Figure 4. Compounds isolated from *Bl. balsamifera* leaves

4. INDONESIAN TRADITIONAL HERBS IN THE FUTURE OF DIABETES TREATMENT

As an integrated part of Indonesian people life, jamu has great potencies as source of novel functional food and lead compounds against diabetes. Authors are currently proposing for jamu development for effective and safe source of alpha glucosidase inhibitors as one possible application in medicinal therapy for diabetes. More basic and advanced researches

are necessary for these Indonesian traditional herbs development to gain clinical acceptance and strength in global market.

REFERENCES

Atta-Ur-Rahman & Zaman, K. (1989). Medicinal Plants with Hypoglycemic Activity. Review paper. Journal of Ethnopharmacology, 26, 1- 55.

Beaglehole, R., & Yach, D. (2003). Globalisation and the prevention and control of non-communicable disease: the neglected chronic diseases of adults. Lancet, 362, 903-908.

Braun, C., Brayer, G. D., & Withers, S. G. (1995). Mechanism-based inhibition of yeast α-glucosidase and human pancreatic α-amylase by a new class of inhibitors 2-Deoxy-2,2-difluoro-α-glycosides. The Journal of Biological Chemistry, 270, 26778-26781.

Campbell, L. K., White, J. R., & Campbell, R. K. (1996). Acarbose: its role in the treatment of diabetes mellitus. The Annals of Pharmacotherapy, 30, 1255-1262.

Ceriello, A. (2005). Postprandial hyperglycemia and diabetes complications: is it time to treat? Diabetes, 54, 1-7.

Chiasson, J. L., Josse, R. G., Gomis R., Hanefeld, M., Karasik, A., & Laakso, M. (2003). Acarbose treatment and the risk of cardiovascular disease and hypertension in patients with impaired glucose tolerance: the STOP-NIDDM trial. The Journal of the American Medical Association, 290, 486-494.

Chung, S. K., Kim, Y. C., Takaya, Y., Terashima, K., & Niwa, M. (2004). Novel flavonol glycoside, 7-*O*-methyl mearnsitrin, from *Sageretia theezans* and its antioxidant effect. Journal of Agricultural Food Chemistry, 52, 4664-4668.

de Padua L.S., Bunyapraphatsara N., & Lemmens R.H.M.J. Introduction. In: de Padua L.S., Bunyapraphatsara N.; Lemmens R.H.M.J. (Eds). (2002). PROSEA 12(1): Medicinal and Poisonous plants.

Diabetes Control and Complications Trial Research Group. (1993). The effect of intensive treatment of diabetes on the development and progression of long-term complications in insulin-dependent diabetes mellitus. The New England Journal of Medicine, 329, 977-986.

Dwek, R. A., Butters, T. D., Platt, F. M., & Zitzmann, N. (2002). Targeting glycosylation as a therapeutic approach. Nature Reviews Drug Discovery, 1, 65-75.

Fogliani, B., Raharivelomanana, P., Bianchini, J. P., Bouraima-Madjebi, S., & Hnawia, E. (2005). Bioactive ellagitannins from *Cunonia macrophylla*, an endemic Cunoniaceae from New Caledonia. Phytochemistry, 66, 241-247.

Gao, H., Huang, Y. N., Xu, P. Y., & Kawabata, J. (2007). Inhibitory effect on α-glucosidase by the fruits of *Terminalia chebula* Retz. Food Chemistry, 105, 628-634.

Gunawan-Puteri, M. D. P. T & Kawabata. (2010). Novel α-glucosidase inhibitors from *Macaranga tanarius* leaves. Journal of Food Chemistry. In press.

Gunawan-Puteri, M. D. P. T., Bhandari, M. R., & Kawabata, J. (2009). Indonesian medicinal plants and their anti-diabetic potencies. In D. M. Martirosyan, Functional Foods for Chronic Diseases, vol. 4 (pp. 110-123). Texas: D&A Inc./FF Publishing.

Hariana, H.A. (2006). Tumbuhan obat dan khasiatnya. 4th ed. Penebar Swadaya, Jakarta

Humphries, M. J., Matsumoto, K., & White, S. L. (1986). Inhibition of experimental metastasis by castanospermine in mice: blockage of two distinct stages of tumor colonization by oligosaccharide processing inhibitors. Cancer Research, 46, 5215-5222.

Karpas, A., Fleet, G. W. J., Dwek, R. A., Petursson, S., Namgoong, S. K., & Ramsden, N. G., *et al*. (1988). Aminosugar derivatives as potential anti-human immunodeficiency virus agents. Proceedings of the National Academy of Sciences of the United States of America, 85, 9229-9233.

Ketzinel, S., Rudi, A., Schleyer, M., Benayahu, Y., & Kashman, Y. (1996). Sarcodictyin A and two novel diterpenoid glycosides, Eleuthosides A and B, from the soft coral *Eleutherobia aurea*. Journal of Natural Products, 59*,* 873-875.

Koop CE. (2002). The future of medicine. Science, 295:233.

Matsui, T., Ueda, T., Oki, T., Sugita, K., Terahara, N., & Matsumoto, K. (2001). α-Glucosidase inhibitory action of natural acylated anthocyanins. 1. Survey of natural pigments with potent inhibitory activity. Journal of Agricultural and Food Chemistry, 49, 1948–1951.

Mehta, A., Zitzmann, N., Rudd, P. M., Block, T. M., & Dwek, R. A. (1998). α-Glucosidase inhibitors as potential broad based anti-viral agents. FEBS Letters, 430, 17-22.

Moco, S., Tseng, L. H., Spraul, M., Chen, Z., & Vervoort, J. (2006). Building-up a comprehensive database of flavonoids based on nuclear magnetic resonance data. Chromatographia, 64*,* 503-508.

Nishioka, T., Kawabata, J., & Aoyama, Y. (1998). Baicalein, an α-glucosidase inhibitor from Scutellaria baicalensis. Journal of Natural Products, 61, 1413–1415.

Paramapojn, S. Ganzera, M., Gritsanapan, W., & Stuppner, H. (2008). Analysis of naphtoquinone derivatives in the Asian medicinal plant *Eleutherine americana* by RP-HPLC and LC-MS. Journal of pharmaceutical and biomedical analysis, 47, 990-993.

Robinson, K. M., Begovic, M. E., Rhinehart, B. L., Heineke, E. W., Ducep, J. B., & Kastner, P. R. *et al*. (1991). New potent α-glucohydrolase inhibitor MDL 73945 with long duration of action in rats. Diabetes, 40, 825-830.

Sakar, M. K., Sohretoglu, D., Ozalp, M., Ekizoglu, M., Piacente, S., & Pizza, C. (2005). Polyphenolic compounds and antimicrobial activity of *Querchus aucheri* leaves. Turkish Journal of Chemistry, 29*,* 555-559.

Satake, T., Kamiya, K., Saiki, Y., Hama, T., Fujimoto, Y., Endang, H., & Umar, M. (1999) Chromone *C*-glycosides from *Baeckea frutescens*. Phytochemistry, 50, 303-306.

Shibuya, H., Fukushima, T., Ohashi, K., Nakamura, A., Riswan, S. & Kitagawa, I. (1997). Indonesian medicinal plants. XX. Chemical structures of eleuthosides A, B, and C, three new aromatic glucosides from the bulbs of *Eleutherine palmifolia* (Iridaceae). Chemical & Pharmaceutical Bulletin, 45, 1130-1134.

Tabata, H., Katsube, T., Tsuma, T., Ohta, Y., Imawaka, N., & Utsumi, T. (2008). Isolation and evaluation of the radical-scavenging activity of the antioxidants in the leaves of an edible plant, *Mallotus japonicus*. Food Chemistry, 109, 64-71.

UK Prospective Diabetes Study (UKPDS) Group. (1998). Intensive blood-glucose control with sulphonylureas or insulin compared with conventional treatment and risk of complications in patients with type 2 diabetes (UKPDS 33). Lancet, 352, 837-853.

Vetrichelvan, T., Jagadeesan, M., & Uma Devi, B. A. (2002). Antidiabetic activity of alcohol extract of *Celosia argentea* Linn. seeds in rats. Biological & Pharmaceutical Bulletin, 25, 526-528.

Yoshikawa, M., Morikawa, T., Matsuda, H., Tanabe, G., & Muraoka, O. (2002). Absolute stereostructure of potent α-glucosidase inhibitor, salacinol, with unique thiosugar sulfonium sulfate inner salt structure from *Salacia reticulata*. Bioorganic & Medicinal Chemistry, 10, 1547–1554.

Zitzmann, N., Mehta, A. S., Carrouee, S., Butters, T. D., Platt, F. M., & McCauley, J. *et al*. (1999). Imino sugars inhibit the formation and secretion of bovine viral diarrhea virus, a pestivirus model of hepatitis C virus: implications for the development of broad spectrum anti-hepatitis virus agents. Proceedings of the National Academy of Sciences of the United States of America, 96, 11878-11882.

RECENT PEAT FIRE TREND IN THE DEVELOPED PEAT SWAMP FOREST OF MEGA RICE PROJECT AREA, INDONESIA

Erianto Indra Putra[1], Hiroshi Hayasaka[2] and Hidenori Takahashi[3]

[1]Silviculture Department, Faculty of Forestry, Bogor Agricultural University, Bogor, Indonesia.
[2]Graduate School of Engineering, Hokkaido University, Sapporo, Japan
[3]Hokkaido Institute for Hydro-climate, Sapporo, Japan

ABSTRACT: Forest fire in Indonesia is not a new phenomenon, but recent fires in logged-over forest, peatland, and plantation should be classified into one of human-made disasters. Fires in Indonesia are more pronounced in El-Nino years, but the recent forest and peat fires in Indonesia tend to occur every year in the dry season, even in non-El Nino years. To clarify this recent fire trend, the Mega Rice Project (MRP) area, Central Kalimantan where large scale development of tropical swamp-forest has been carried out since 1996, selected as the study area. To identify trend of the recent severe peat fires, weather data in Palangkaraya, hotspot data captured by the NOAA and MODIS satellites, monthly sea surface temperature (SST) anomalies, and ground water level (GWL) data were analyzed. The analysis results clearly show a relationship among fire occurrence trend, the precipitation pattern of the dry season, GWL change, and SST Anomalies. Peak fire period started in the middle of August when daily precipitation reached the minimum and GWL had steep decreasing trend. Active fire period lasted under low GWL less than -40 cm, suggesting that critical level for peat fire can be considered at around -40 cm. Recurring large fire occurrences in the MRP area, even in non-El-Nino year, indicates that recently even low positive SST Anomalies more than $+0.3^0$C may result to high number of fires in MRP area. The above results suggest that large areas of bared peat in the MRP now has a high susceptibility to fire coupled with the precipitation pattern change of the dry season related to SST Anomalies; implying that peat fire trend in the MRP area is simply related to local peat dryness there. A detailed hotspot distribution map shows that large areas of MRP (Blocks A and C) on deep peatland still have high fire densities due to ongoing human disturbance. Severe fire areas in MRP are in open area, supporting that fires were mainly human-caused fires due to intentional and careless use of fires.

Keywords: *Peat fire, Sea Surface Temperature anomalies, Hotspots, Ground Water Level, Mega Rice Project*

I. INTRODUCTION

In 1996, the Indonesian Government initiated the Mega Rice Project (MRP) in Central Kalimantan to convert one million hectares of peatland between Sebangau and Barito rivers to fields for cultivating rice and promoting transmigration (migration inside of Indonesia). The MRP closed at 1999 but it left vast drained peatland mainly due to the built of the channels to open up this area and make it suitable for cultivation. Frequently large fire occurrences in MRP area is believed released huge amounts of carbon dioxide to the atmosphere. Around 4,740 km2 area in MRP has been damaged from severe fire episodes in 1997 and released 0.19 – 0.23 Gt of carbon to the atmosphere [1].

More than 90% of peat fires in Central Kalimantan from 1997 to 2007 occurred in dry season. Ground Water Level (GWL) in peatland area is getting lowered under dry weather condition, dry up peat and organic fuel in its upper layer and creates suitable condition for fires to be ignited. Main goal of this study is to gain better understanding on the peat fire trend in the

MRP area and underlying it causes and impacts. To achieve this, objectives of this study were as follows: (1) to understand how drought and peat fires were related in the MRP area through daily hotspot and weather data analysis, (2) to investigate the relationship among precipitation pattern in the dry season, SST Anomalies, ground water level and peat fire trend in the MRP, and (3) to identify the most affected areas from peat fires and to assess the burnt area in MRP.

2. METHODOLOGY

Analysis is done for daily hotspots data captured in MRP area by SiPongi-NOAA and NASA-MODIS satellite, daily precipitation and SST anomalies data to clarify the relationship among SST anomalies, precipitation and peat fire occurrences. Precipitation and hotspots data are processed by using five-days moving average to obtain their smoothed daily and seasonal pattern. Ground water level (GWL) is modeled from data measurement done by Takahashi *et al.* [2]. Mapping of hotspots using 3,117 grids of 1 km^2 by using ArcView is done to determine where the worst fire occurred in the MRP.

3. RESULTS AND DISCUSSIONS

3.1 Recent hotspot (fire) trend in Kalimantan and Sumatra

Fires in tropical forest and peat area in Indonesia are not new phenomenon. Recently forest and land fires in Indonesia have become commonplace and occurred every year. Unfortunately, the old fires history data in Indonesia is not documented well. Official reports on burned forest areas provided by the Ministry of Forestry of Indonesia became available only from 1984. In other hand, the daily satellite data detection was available only from July 1997 when the Ministry of Forestry (MOF) and Japan International Cooperation Agency (JICA) started hotspot detection using NOAA-AVHRR satellite for the western part of Indonesia. From the end of 2000, MODIS satellite from NASA/FIRMS started to detect hotspots in Indonesia. However, the complete fire datasets from NASA/FIRMS were available from 2001.

Fig. 1 showed recent Indonesian forests burns and the number of hotspots detected in western Indonesia by NOAA-AVHRR satellite from the Japan International Cooperation Agency Forest Fire Prevention Management Project (JICA-FFPMP) – SiPongi. The hotspots data in Fig. 1 covers Sumatra, Kalimantan, Java, Bali, and Sulawesi Islands.

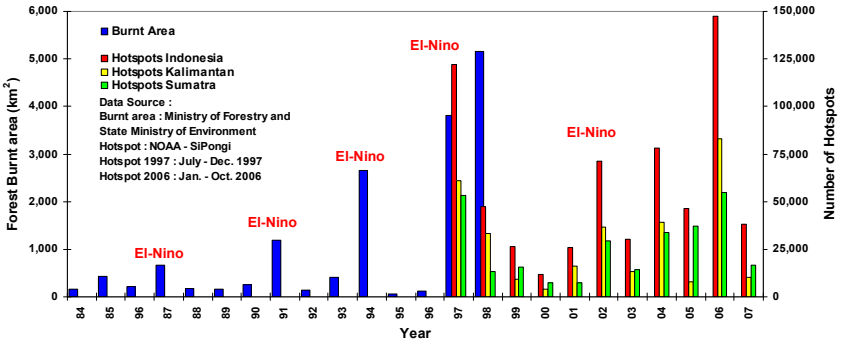

Fig. 1 Forest burnt area and number of hotspots detected by SiPongi-NOAA, 1984 – 2007

Over 1,000 km^2 of forest area burned in 1991, 1994, and 1997, with the highest in 1998. Over 60,000 hotspots or Indonesian fires were recorded in 1997 and 2002 or in El-Nino years brought the evidence of the close relationship between fire and El-Nino event. However, recently large number of fires also found in Non El-Nino year such as in 2001, 2003, 2004, 2005, and 2006. The highest number of hotspots is found in 2006 (147,731), made 2006 as the worst fire year since 1997. These findings strongly suggesting that recently fire in Indonesia has become yearly occurrences and not only El-Nino event any more.

3.2. Recent hotspot (fire) trend in MRP area

The smoothed mean daily precipitation curve shows a U-shaped precipitation pattern in Palangkaraya (Fig. 2). A daily mean precipitation (7.84 mm) is used to differentiate the dry and wet seasons in Palangkaraya. The wet season lasts about seven months and it is two months longer than the dry season. The length of the dry season is about five months from the start of June (DN 152) to the end of October (DN 301). Thus, this study defines June to October as the dry season in Palangkaraya.

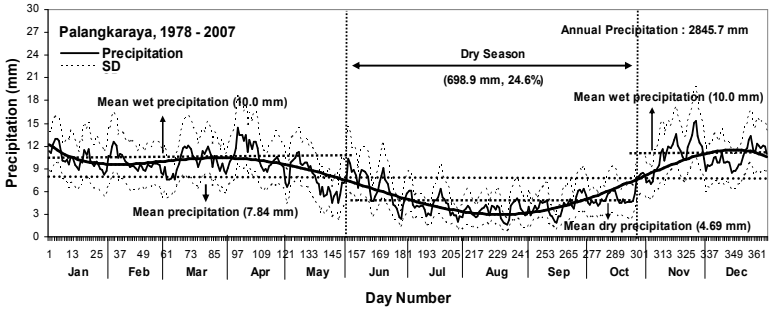

Fig. 2 Daily precipitation cycle in Palangkaraya

The precipitation pattern in Fig. 2 clearly shows the large difference in precipitation between the wet and dry seasons in Palangkaraya. There is a more than two times difference between the mean daily precipitation values in the dry season (4.69 mm) and wet season (10.0 mm), and the total precipitation in the dry season (698.9 mm) is only 1/3 of that in the wet season, this pattern clearly describes the overall dry climate conditions in Palangkaraya during the dry season.

Low daily precipitation, less than the mean dry precipitation (4.69 mm), occurred between July and September and the lowest daily precipitation of less than 3 mm is in the middle of August. Low precipitation brings a drier climate and increases the dryness of the peat in the MRP area. Thus, based on the data here we suggest the middle of August as both the peak of the dry season as well as the start of the peak of the fire season.

There was a negative correlation between SST Anomalies and precipitation in Palangkaraya in July – October, 1978 - 2006 (Fig. 3), indicating that the drought in Palangkaraya is proportional to positive SST anomalies. The of more than +0.5^{0}C SST Anomalies bring less than 400 mm precipitation in July – October such as in 1997, 1991, 2004, 2006, 1982, 1987, and 2002. However, below mean value precipitation also occurred in several neutral or non El-Nino years such as in 2003, 2004 and 2005, when there were low positive SST Anomalies between +0.1^{0}C and +0.5^{0}C. This may indicate that recently even low positive SST Anomaly occurrences may bring on severe dry conditions in Palangkaraya.

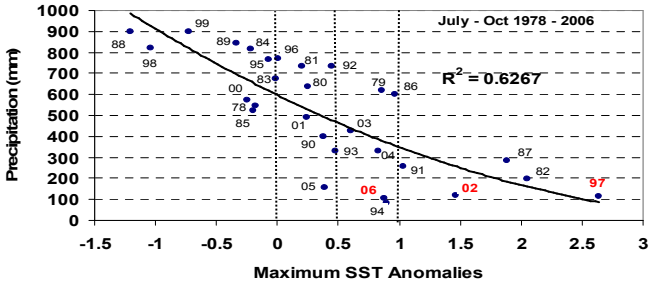

Fig. 3 Correlation between SST Anomalies and total precipitation in July - October, 1978 – 2007

Dry climate during dry season may dry up above ground fuel and peat and increasing its flaming risk. Over 90% of hotspots in the MRP area from 1997 to 2007 (Fig. 4) occurred between July and October or during the dry season. High numbers of hotspots were detected primarily in the dry seasons with high positive SST Anomalies. The SiPongi-NOAA captured 8,401 hotspots in 1997, 4,961 in 2002, 3,591 in 2004, and 5,734 in 2006, when high positive SST Anomalies enhanced longer dry periods. In these years fire events peaked in August, September, and October, when the area had precipitation below 100 mm.

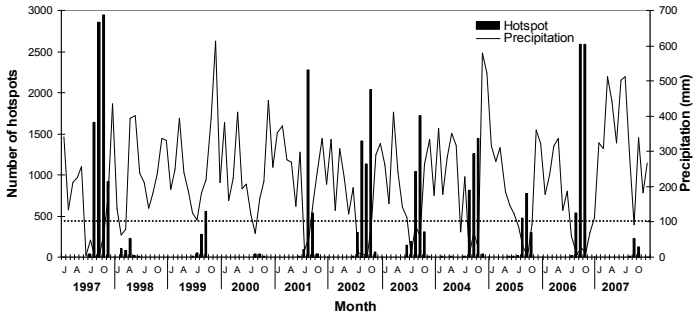

Fig. 4 Precipitation and hotspot occurrences in the MRP area from 1997 – 2007

High numbers of fires, however, also occurred in the dry seasons of 2001, 2003 and 2005; when positive SST anomalies were low suggesting that fire occurrence is associated with droughts as indicated by positive SST anomalies. Therefore peat fires in the MRP area are no longer limited to El Niño years.

Strong relationship (R^2=86.42%) is found between the number of hotspots and positive SST anomalies in July to October in 1997 to 2007 (Fig. 5). Positive SST anomalies thus clearly induced high numbers of fires. The highest number of hotspots occurred during the 1997 following the highest SST anomalies in this year. A relatively high number of fires were observed also, however, in non-El Niño years with positive SST anomalies, i.e., in 2001, 2003, and 2005. Over 1,500 fires occurred in these years when SST anomalies exceeded +0.3^{0}C, indicating that recently even low positive SST Anomalies yield high numbers of fires.

Figure 6 shows that the peat fire occurrence in the MRP area coincides with the precipitation curve. Daily precipitation decreased gradually from June and reached the lowest point in the middle of August, creating the necessary dry conditions for fires to ignite. Then, fires start to

occur on a daily basis from the middle of June and become numerous from the end of July, making the end of July the start of the fire season in the MRP area. The peak fire period starts from the middle of August when daily precipitation drops below the lowest mean value, less than 3 mm. The fire season ended at the middle of November or about twenty days after the end of the dry season at the end of October. This may indicate that peat in the MRP area is still in the dry condition at the beginning of the wet season, after suffering from the severe dry conditions of the long dry season, thus maintaining the condition where ignition is easy.

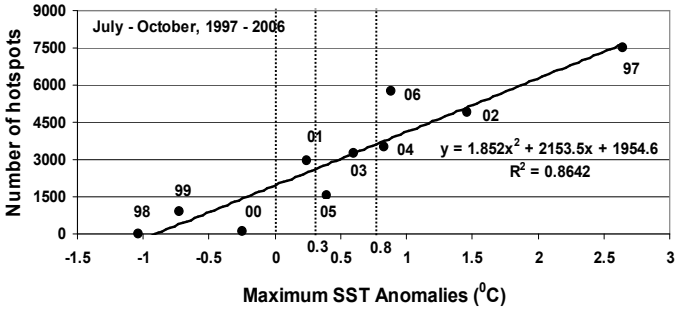

Fig. 5 Relationship between number of hotspots and maximum SST anomalies, July – October 1997-2006

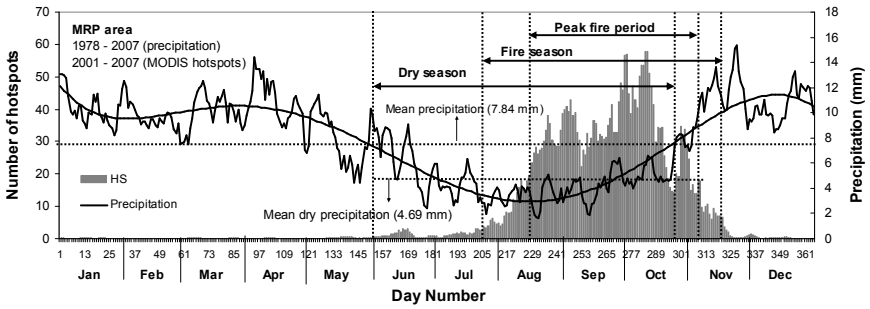

Fig. 6 Daily precipitation and hotspot occurrences trend in MRP area

3.3. Ground water level, precipitation and peat fire occurrence in MRP area

Figure 7 showed the changes in GWL in the MRP area. The GWL stays steady at around 5 cm higher than the soil surface between January and the middle of May, in the wet season; suggests that the area could be categorized as a peat swamp forest area. The GWL decreased progressively below soil surface during the dry season from the end of May until it reached the lowest value in early October; clearly indicating that the GWL followed the precipitation changes. However, there is a time-lag between GWL and precipitation.

There is about a one and a half month time-lag between the lowest precipitation in mid August and the lowest GWL in early October. The decrease of precipitation takes 3 months to reach the lowest in mid August (from mid May), but the lowering of GWL below the soil surface takes around 4.5 months from the middle of May until it reaches its lowest value in early October. The GWL then reaches the soil surface again at the end of December after the precipitation has reached its highest value in mid December. This may suggest that the recovery of the ground water level in the MRP area occurs after having been replenished by the water supplied by the continuous precipitation.

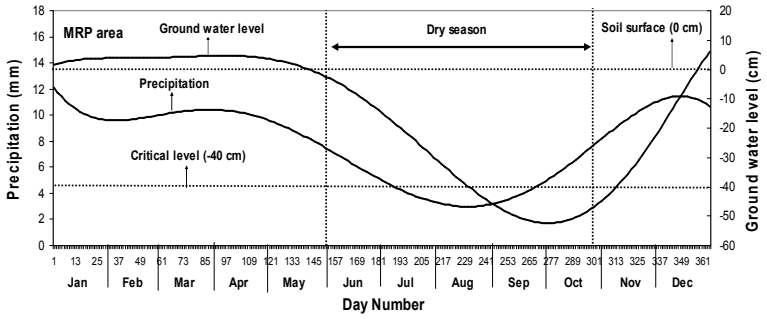

Fig. 7 Ground water level and precipitation changes

Fire occurrences in the MRP area coincide with the GWL (Fig. 8). More than 99% of fires occurred when the GWL was below the soil surface. The peak fire period in the MRP area started when the GWL reached -40 cm in the middle of August and fires become more severe when GWL is below -40 cm from the middle of August till early November. Therefore this study suggests -40 cm as a critical level of GWL for large peat fire occurrences in the MRP area, and this GWL should be used as an indicator for a high likelihood of severe fire occurrences there.

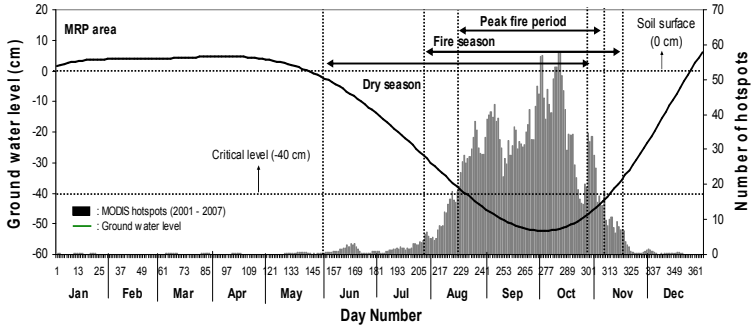

Fig. 8 Ground water level and hotspot occurrence in MRP Area

The decreases of GWL clearly indicated that in recent years GWL in the Mega Rice Project (MRP) area became very deep mainly in the dry season. Therefore peatlands were in severely dry conditions in the dry season and this creates a situation where ignition and combustion is promoted, and the large number of fires that occur while the ground water level is low in the dry season substantiates this.

3.4 Peat fire distribution and density

In order to find the most dense areas from peat fire, local MRP area fire density of 1 x 1 km grids is calculated based on NASA-MODIS daily hotspot data from 2001 to 2009 (Fig. 9). Number of hotspots/km^2 is used as a unit for fire density. Almost all areas were affected by fires, with the highest fire density in the southern part of Block C and upper part of Block A. High fire density was also observed along channels in Blocks C and B, central part of Block A and near main drainage channels in Block A and B. Recurring fires in these areas resulted to the high fire density.

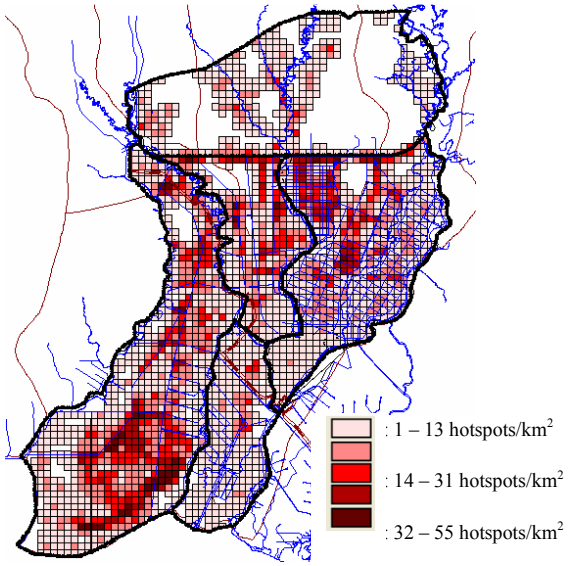

Fig. 9 Hotspot (fire) density in MRP area from 2001 – 2009

High hotspots density of more than 32 hotspots/km^2 during 2001 – 2009 was found along the canals in southern part of Block C, paddy fields in Block A and along primary channel in Block A and B. Southern part of Block C is dominated by high hotspot density of more than 53 hotspots/km^2 as well as along Trans-Kalimantan highway road and along canals in northern and eastern part of study area. Less hotspots density was found in forest area of Block E.

There were many agricultural field and abandoned farmland found along the canals as well as along Trans-Kalimantan highway road. The fact that these high-fire-density areas mainly involve paddy fields and abandoned farmland, mostly located near channels, suggests that using fire in land preparation and slash-and-burn activities in the dry season still continuing. Thus, as the peat fires here are human-caused fires, peat fire in MRP must be prevented by reducing both intentional and careless fire use. This requires that people in MRP area communities must be trained and their awareness of fire prevention and fire extinguishing must be raised.

4. CONCLUSIONS

Hotspot (fire) data, daily weather data, SST Anomalies, and ground water level data were analyzed in this study to clarify recent peat fire trend in the Mega Rice Project (MRP) area. The results of this study are summarized as follows:

1. This study clearly showed that large areas of bared peat in the MRP area now are highly susceptible to fires. Recent trend of hotspot (fire) showed that many hotspots (fires) found in bared peatland in MRP area after MRP development. Most of hotspots (fires) were occurred in dry months of August to October from 2001; indicating the couples of dry season and peat fire trend in MRP area.
2. The daily precipitation analysis using 30 years weather data from 1978 to 2007 clearly showed that Palangkaraya has seven month wet season and five months dry season that starts from early of June and ends at the end of October. About two times difference

between mean precipitation values in the dry and wet season was also found. Mean daily precipitation less than 3 mm were found in August or in the middle of dry season, suggesting the middle of August as the peak of the dry season as well as the start of the peak fire period. Under this precipitation pattern, dryness of peat is increased and stimulated the large number of fire occurrences.

3. Peat fire in MRP area is found more pronounced in El-Nino years, but number of fires exceeded 2,500 in non-El-Niño year with positive SST anomalies in 2003 and 2005; indicates that recently even low positive SST Anomalies more than $+0.3^0$C may result to high number of fires. Thus, SST Anomalies may more precisely relate to fire trend in MRP area instead of El-Nino event.
4. The peak fire period coincided with low GWL less than -40 cm, suggesting around -40 cm as a critical level for peat fire occurrence. Thus, -40 cm of GWL could be used as an alarm for the severe peat fire occurrence in the MRP area. .
5. A detailed hotspot distribution map showed that large area of Blocks C and A in MRP seriously damaged by peat fires. Their percentage of fire-affected area to total block area during 1997 – 2009 reached 73.9% in Block C and 74.6% in Block A. High peat fire density are found in agricultural fields, abandoned lands and along canals and roads, suggesting that intensive ongoing human activity accelerates fire occurrences in MRP. Thus, this situation allows us to classify peat fires here as one of man-made disasters.

ACKNOWLEDGEMENTS

The authors are very grateful to Ms. Minnie Wong, University of Maryland, Fire Information for Resource Management System (FIRMS) of U.S for providing the MODIS fire datasets.

REFERENCES

[1] Page SE, Siegert F, Rieley JO, Boehm H-DV, Jaya A, Limin S. 2002. The amount of carbon released from peat and forest fires in Indonesia during 1997. Nature Vol. 420, pp. 61 – 65, 2002.

[2] Takahashi H, Usup A, Hayasaka H and Limin SH. 2007. Overview of hydrological aspects for recent 10 years in the basins of River Sebangau and Kahayan. Environmental Conservation and Land Use Management of Wetland Ecosystem in Southeast Asia. Annual Report for April 2006 – March 2007, pp. 141 – 144.

[3] Usup A, Hashimoto Y, Takahashi H, Hayasaka H. 2004. Combustion and thermal characteristics of peat fire in tropical peatland in Central Kalimantan, Indonesia. Tropics Vol. 14 (1) 2004 : 1-19.

[4] Hooijer A, Silvius M, Wosten H, Page SE. 2006. Peat-CO2: Assessment of CO_2 emission from drained peatlands in SE Asia. Delft Hydraulics Report Q3943 (2006).

[5] Putra EI, Hayasaka H, Takahashi H, Usup A. 2008. Recent peat fire activity in the Mega Rice Project area, Central Kalimantan, Indonesia. Journal of Disaster Research Vol. 3 No. 5 (2008), pp. 334 – 341.